ALMA MATER STUDIORUM - UNIVERSITÀ DI BOLOGNA

DOTTORATO DI RICERCA IN

INGEGNERIA DEI MATERIALI

CICLO XXIV

Settore concorsuale di afferenza: Scienza e Tecnologia dei Materiali (09/D1)
Settore Scientifico Disciplinare: Scienza e Tecnologia dei Materiali (ING-IND/22)

SUSTAINABLE INORGANIC BINDERS AND THEIR APPLICATIONS IN BUILDING ENGINEERING: A GREEN ALTERNATIVE TO ORDINARY PORTLAND CEMENT

Presentata da

Ing. Annalisa Natali Murri

Coordinatore Dottorato

Prof. Giorgio Timellini

Relatore

Prof. Maria Chiara Bignozzi

Correlatori

Prof. Arie van Riessen

Prof. Franco Sandrolini
Dott. Stefania Manzi

Esame finale anno 2012

To my parents

Summary

Research aim

More than in any other field of industrial research, the context of building materials and construction industry is starting to feel the need to develop green materials and technologies with low or null environmental impact. The building sector, indeed, has one of the greatest impacts on our environment and measures have to be taken to limit the use of non-renewable resources.

The aim of this thesis is therefore to study and evaluate sustainable alternatives to commonly used building materials, mainly based on ordinary Portland Cement (OPC), and find a supportable path to reduce CO_2 emissions and promote the re-use of waste materials.

More specifically, this research explores different solutions for replacing cementitious binders in distinct application fields, particularly where special and more restricting requirements are needed, such as restoration and conservation of architectural heritage. Emphasis was thus placed on aspects and implications more closely related to the concept of non-invasivity and environmental sustainability.

A first part of the research was addressed to the study and development of sustainable inorganic matrices for continuous carbon fiber reinforced materials in structural rehabilitation. Innovative systems have been developed consisting of woven carbon

fabrics pre-impregnated with an inorganic polymer-added matrix, with the aim to promote a better adhesion to the substrate and facilitate their installation. A traditional green binder, such lime putty, was chosen in place of the more commonly used Portland cement to formulate the matrix: a less intrusive and more compatible strengthening system was hence obtained and, as such, particularly suitable for intervention on historical substrate materials.

The research was thus directed to the study of new sustainable inorganic binders, based on alkali-activation. High-performance binders with specific requirements and properties were thus developed, and innovative materials, suitable to be used in repair interventions and other critical operating conditions, were formulated.

With the aim to further limit the exploitation of non-renewable resources, a relevant issue that was therefore taken into account was to optimize the reuse of waste materials deriving from industrial processes. The synthesis of chemically activated silico-aluminate inorganic materials from ladle slag and fly ash was hence successfully achieved and new sustainable binders were proposed as novel building materials, as primary component for construction and repair mortars or as matrices for fiber reinforced composites.

The research project was developed at the Department of Civil, Environmental and Materials Engineering (DICAM) of the University of Bologna and, for a period of six months, at the Centre for Materials Research of Curtin University of Technology (Bentley, Perth, Western Australia).

1 Introduction

1.1 Ordinary Portland Cement: environmental costs and drawbacks

Globally, widespread agreement has been reached that the threat of climate change is real and global actions need to be taken to reverse the increasing trend of global greenhouse gas emissions. OPC based concrete is one of the largest artificial source in the world in the production of carbon dioxide. Its production process, starting from cement manufacturing, counts at least 5 to 8% of CO_2 emissions into the atmosphere each year. The European industry represents about 10% of cement world production and is therefore a key sector to focus on to reduce emissions. Therefore, OPC production, as it is one of the most energy intensive industrial sectors, has a great potential to significantly reduce the CO_2 footprint. Currently the production of one ton of cement commonly results in the release of 650-690 kg of CO_2, depending on the efficiency of the process and used fuels [1]. Typically, around 55% of the CO_2 emissions in the production of cement originate from clinker production process (limestone decarbonation that is conversion of $CaCO_3$ into CaO). Around 40% of the emissions results instead from the combustion processes needed to yield the thermal energy required for this reaction, that takes place at 1450°C [2]. Projections show that demand for cement could arrive in 2030 to a level five times higher than in 1990, reaching a

value of five billion tons, as estimated on the basis of the study data produced by the European Cement Association [2]. The European cement industry, besides having the responsibility to ensure that a sufficient amount of cement is produced to meet the manufacturing needs, shall now primarily aim to reduce the consumption of natural resources, fossil fuels and CO_2 emissions. Therefore, the building industry and scientific research should focus on promoting the use of alternative fuels and develop new valid OPC substitutes.

As regards concrete production, a possible attempt that can be made to reduce carbon emissions may also consider recycling of fine and coarse aggregates, as they contribute approximately 30% of all emissions during the production of concrete [3]. However, remarkable emission reductions can be obtained when a high carbon footprint material or process is substituted for a lower one [4]. Moreover, it is worth to note that at least as regards developing countries, such as China and India, the demand for OPC-based concrete is thought to remain rather high for the next years and cement industries are still expected to expand significantly. OPC will hence continue to have strong market dominance, especially as long as no solid guidance directions on the use of alternative binders can affect significantly any market choice. The development of new sustainable binders as substitutes for OPC is hence currently representing an outstanding goal to achieve and strategies to make them a technically and economically viable option, supported from the market industry, is becoming increasingly unavoidable [4]. An affordable and relatively easy path to reduce greenhouse emissions could be represented by simply substituting cement with other alternative cementitious materials, as ground granulated blast furnace slag, coal fly ash, pozzolanic ash or silica fumes. By now, this is most commonly achieved by blending the cement with one or more pozzolanic materials, defined as materials which can react with the calcium hydroxide ($Ca(OH)_2$)

formed during cement hydration to produce cementitious binding phases.

1.2 Traditional sustainable binders: hydraulic lime

Alongside the development of modern materials that have being studied to support environmental sustainability, another viable path has being considered to reduce carbon footprint of construction energy on our environment. A marked revaluation of traditional eco-friendly building materials may lead as well to promising solution in terms of lower CO_2 emissions and natural resources conservation. Natural binders, as for example hydraulic lime and lime putty, can successfully be used in several application fields, like restoration and historical building conservation, residential and bio-architecture. Lime, indeed, is a green and sustainable product: it is produced by firing of limestone (800-1000 °C) that, subjected to intense heating, decomposes into calcium oxide (CaO, or lime), releasing carbon dioxide in the measure of 785 g for each kg of quicklime obtained [5]. During use, the lime firstly reacts with water (hydration) to give rise to hydrated lime; then, once placed on site in the form of mortars, plasters, paints, it absorbs the same amount of CO_2 from the air (carbonation), reconverting into calcium carbonate. Its lifecycle represent an example of environmental sustainability, except for the release of CO_2 into the atmosphere due to the use of fossil fuels to power the kilns. By now, the caloric intake theoretically needed to produce 1 kg of lime is 764 calories, but energy actually required is much greater, because of the effective carbon fed kilns efficiency. However, in terms of energy efficiency and carbon emissions, the production of lime is surely more sustainable than that of OPC, both for the total emitted CO_2 during production process and, especially, for its ability to subtract carbon dioxide from

the atmosphere after its setting up onsite. Lime has many properties that contribute to make it a green building material, as it is a natural binder, produced just by limestone firing; it does not contain or release harmful substances for human health nor for the environment, in most cases subtracting them from the environment by means of simple chemical reactions. It is also diffused almost everywhere and can be produced locally, without any additional transportation cost, thus contributing to make it a low cost and sustainable building material. Another relevant issue that should be taken into account when comparing lime to traditional OPC binders is given by the absence of potentially detrimental chemical compounds, such as tricalcium aluminates and soluble alkalis, that are naturally present in cementitious binders: this feature significantly contributes to improve the durability of lime mortars and pastes, making them immune to the destabilizing action of sulphates and the deleterious reaction alkalis-silica [5].

By now the use of lime and lime putty is pretty much confined to interventions on the historical architectural heritage, where cementitious binders have been permanently banned, but much work still has to be done in the years to come to integrate its use in new construction and other application fields as well.

1.3 Innovative sustainable binders: geopolymers and alkali activated materials

An innovative class of eco-friendly binders based on alkali activation can represent an interesting solution to natural resource exploitation and can significantly reduce carbon footprint on our environment. Binders deriving from chemically activation also called geopolymers or alkali-activated materials (AAM), thanks to their synthesis procedures that involve lower process temperature, have a great potential to lower CO_2 emissions.

These materials can be considered as effective innovative inorganic binders, suitable to act as OPC replacement in different application fields, thanks to their excellent properties and features. Depending on the raw material selection and processing conditions, geopolymers can exhibit a wide variety of properties and characteristics. Compared to OPC, geopolymers in fact exhibit a good volume stability, showing a shrinkage about 4-5 times lower, a reasonable strength gain in a short time, obtaining up to 70% of the final compressive strength in the first 4 hours of setting, an excellent durability, as they can stand weathering attacks without any excessive function loss, an high fire resistance and an outstanding high temperature behaviour, as they can easily withdraw temperatures in the range of 1000-1200°C [6].

The raw materials that can undergo a geopolymerization process are characterized by high silica (SiO_2) and alumina (Al_2O_3) content, which are widely present in most of natural minerals, as well as in several waste materials and industrial by-products. The absence of lime-based starting materials, together with a definitely low process temperature (the calcining temperature for a commonly used kaolin clay is about 700°C, versus 1450°C required from clinker production) suggest that geopolymers production

can be considered more sustainable compared to that of OPC, because of a sensible reduction in CO_2 emissions. Moreover, besides these outstanding advantages deriving from a different and more sustainable production process, the development of geopolymer and alkali activated binders or materials should give the chance to set up a new generation of high performance materials for structural rehabilitations.

Geopolymers started to seriously attract the interest of scientific research in the 70s, as Davidovits and Glukhovsky [7,8] investigated the differences that define ancient cementitious systems from modern concretes, thus developing various inorganic alumino-silicate binders from several distinct materials (clays, feldspar, volcanic ashes and slags) [9]. The term "geopolymer" usually indicates a chemically obtained silico-aluminate based material, formed by the reaction of a solid alumino-silicate with a highly concentrated aqueous alkali hydroxide or silicate solution. Depending on the starting materials that are involved in the synthesis reaction, the amorphous to crystalline formed product can be more generally referred to as alkali-activated material (AAM). Though the synthesis process that regards the raw silico-aluminates and some macroscopic properties of the reaction products may be the same, the alkali-activated materials that can be derived are commonly defined by different microstructures and widely distinct physical, mechanical, chemical or thermal properties [10].

Basically, dissolution of the solid alumino-silicate source by alkaline hydrolysis results in the release of aluminate and silicate species. These species, after dissolution, are included into the aqueous phase, that may be itself enriched with other silicate species from the activating solution, thus creating an heterogeneous mixture of silicate, aluminate and alumino-silicate species. Differently than hydration process of common cementitious materials, the water, as a reaction medium, does not really take part in the formation of the gel and is released during the process, lying within the pores of the gel.

The system continues than to rearrange and reorganize after gelation, as the connectivity of the gel network increases, resulting in a three-dimensional alumino-silicate network that commonly defines the hardened structure of geopolymers [10].

Geopolymers and alkali-activated materials represent an alumino-silicate binding system that has been known since late 60s. So far they have never been produced in wide quantities for industrial applications, except for some significant applications that involved small amounts of geopolymer together with ordinary cement to set up concrete mixtures [11].

During the past years, the development of basic mix formulations for geopolymers as bulk building materials was preceded by an intensive raw material screening, to asses the suitability of natural minerals and waste by-product to react and harden under highly alkaline environment. So far one of the most promising and widely adopted material used to formulate geopolymers was metakaolin [12-14]. However, although some interesting technical perspectives presented by its utilization, metakaolin was found not to have the required properties to act alone as a main binder component for producing bulk building materials, especially because of its economic and ecological deficiencies. Indeed, although metakaolin reactivity is largely better than that of other raw materials and, as such, should be regarded as an optimum precursor, other alumino-silicate are by now generally preferred for geopolymerization [15]. Metakaolin powder, in facts, generally has a high specific surface and, for that, requires wide amounts of water to make properly workable mixtures. Therefore, long curing times and higher temperatures (60-80°C) are needed for the complete removal of un-bonded water from the geopolymer structure. Therefore, industrials wastes and other unexploited low-impact silico-aluminate raw materials were also considered as possible primary sources for geopolymers. As for the industrial wastes, since they require a smaller amount of water

in the mixtures, are more suited to a fast setting even at room temperatures. For example particular attention was paid to fly ash particles that derive from coal combustion and are formed in the furnace then rapidly quenched in air, thus acquiring a peculiar glassy and spherical structure. This particle shape gives fly ash the ability to reduce the water demand in the mixtures, thus maximizing particle packing and reducing porosity. However, fly ash usually contains different amorphous or crystalline impurities, such as calcium and iron oxides or quartz that can significantly vary their reactivity and the resulting properties of hardened material, depending on their nature. Class F fly ash, the most widely used to produce geopolymers, is characterized by extremely low amounts of Ca, while higher contents are present in Class C fly ash, which is, for this, less used [15, 16]. The calcium content that may be present in precursor materials can, in facts, affect more than other secondary element the microstructural properties of the material, possibly because of the rapidity with which setting may occur for these mixtures. Free calcium oxide generally also promote the formation of various silico-aluminate calcium-based compounds within the geopolymeric gel, thus leading to a more heterogeneous and complex material. Metallurgical slags (ladle slags or ground granulated blast furnace slags) can also be successfully activated with alkaline solutions. Slags from iron or steel production, whose composition is basically that of an over-charge-balanced calcium alumino-silicate framework [15], can be regarded as an highly impure silico-aluminate, as calcium oxide content can reach 40% and more of the overall composition of the material. For this reason, some forms of C-S-H phases, which is well known that contribute for most of the mechanical strength in OPC systems, can be detected as reaction products in Ca-enriched alkali-activated materials, coexisting with the alumino-silicate polymer network [17]. Alkali activated blast furnace slag, fly ash and blast furnace slag or metakaolin blends can hence exhibit similar or better properties than

OPC systems in term of strength, lower shrinkage and higher chemical durability, as shown by previous research works [18-20].

Alkali-activation can thus represent a viable solution to the search for possible ways of re-utilizing large amounts of ash and slag produced, especially for those countries that have not yet developed any adequate ways of re-using industrial wastes. It can be clearly seen how alkali-activated binders and geopolymers could this way prevent the large-scale land filling of ash and slag, with a corresponding conservation of primary non-renewable raw materials [21].

As regards an expected better and more sustainable behaviour of geopolymers as for greenhouse emissions, although many studies argued that cement production can result in a CO_2 emission rate up to 6 times higher than that of geopolymers, a real comparison cannot be done so easily, at least unless other relevant factors are not taken into account. Important issues that should be considered before making any comparison between OPC and geopolymer binders are mainly relative to transportation and production costs of the chemical reagents involved in the process, as they can affect significantly or even null the environmental benefits that can be achieved, especially for small-scale productions [22].

2 Green binders application fields

2.1 Construction, bedding and repair mortars for architectural restoration

The steady growth of architectural restoration and rehabilitation and the associated need for materials capable to ensure compatibility and coherence with the original substrate materials and construction technique strongly contributed to ensure that the use of traditional binders was not completely abandoned. Moreover, the increased attention that is being paid to environmental impact and related issues in the field of construction industry is promoting solutions that best harmonize with the existing built environment. For these reasons, traditional sustainable binders, as lime or lime putty, are still catching the interest of scientific research, just like innovative and experimental ones obtained by alkali-activation.

Lime pastes and mortars are used for several distinct applications, among which the most significant are relative to heritage conservation. Generally, the use of lime-based formulations for mortars (bedding mortars for masonry structures and construction mortars), plasters and finishing results in several advantages, such as ensuring the adequate transpirability to the substrates and promoting a good adhesion to the support material, as the nano-sized particles, especially in lime putties, are able to penetrate deeper into the substrate's porosity. As for consolidation interventions, lime is for example used in historical masonry or stone walls consolidation and plasters integration. Inorganic lime injection mixtures are used indeed when diffuse lesions and relatively high percentages of internal cavities affect the substrate. The consolidating

mixture should physically be able to penetrate toward the damaged structure and to improve mechanical properties of the substrate by eliminating the cavities (cracks or voids) and reinforcing connections between the substrate material's components. As such, lime injection mixtures for consolidation result a widespread intervention solution for historical buildings, where a prerequisite is to maintain the original appearance and structure for the structure. Lime grouts thus have the advantage of retrieving the continuity, cohesion and strength of the damaged structures without altering their morphology and load-bearing system. Hydraulic lime-based grouts (hydraulic lime with or without a pozzolanic material) seem hence to offer a promising alternative to cementitious grouts, due to their similarity with the original materials in terms of mechanical and physical properties (compressive strength, elastic modulus and thermal expansion coefficient) and their global efficiency for stone and masonry walls structural rehabilitation [23, 24]. Lime is generally used in the form of lime putty, because of its better ability to penetrate the substrate, and is efficiently spread inside the walls. However, it presents a relatively high shrinkage and the possibility of coarse grains to occlude the holes, causing water stagnation and possible damages in case of freeze-thaw cycles, may occur. An appropriate addition with opportune fillers, to cope with the above mentioned drawbacks, may allow more efficient and satisfactory applications. As for bedding mortars, hydraulic lime is increasingly used also for new building constructions. Recent studies performed on natural hydraulic-lime (NHL) mortars demonstrated that they possess adequately high water retention, thus enabling an efficient bond strength that can compare well to that of Portland cement or cement/lime mortars. In facts, bond strength, which may affect significantly the mechanical behaviour of the whole structure, for NHL mortars is found not to be determined by the binder’s hydraulic strength, but increases proportionally to the mortar’s water retention:

the higher the water retention, the strongest the bond [25]. Nevertheless, these mortars can be very important for the conservation of historic buildings where the use of ordinary cement is mostly avoided. Several damage cases are known to have been caused by the use of cement in the conservation of historic buildings because of cement's excessive hardness, stiffness and impermeability. Cement also contains more soluble salts, which may be harmful for historic buildings.

A different operating solution for interventions on historical buildings may involve the use of innovative binders, obtained by alkali-activation. Geopolymers indeed are alkaline silico-aluminates and, as such, they may be regarded as products that meet the compatibility and reversibility requirements if used for restoration of natural or artificial stones, mortars and various types of ceramics. Some literature work [26] did investigate the possibility of using geopolymers for conservation and restoration of historical buildings or artefacts, absolving different functions: adhesive, reinforcing, filling gaps, reconstruction of missing parts, preparation of copies. Experimental tests have already been successfully performed on terracotta elements, confirming the effectiveness of using geopolymers as adhesive for restoration applications, even without specific high-temperature curing treatments [27]. Therefore, the efficacy of the investigated consolidation technique leads us to think that alkali-activated materials may be considered also for interventions on other types of ceramic materials, and used both to formulate adhesive pastes and repair mortars. In facts, the specific physical, chemical and mechanical properties of a geopolymer can be easily designed in advance, to fit the substrate's proper nature, by properly choosing and measuring out each reactive component of the mixture.

Another promising application of alkali-activated materials in the field of stone

conservation may be represented by mechano-chemical activation of natural precursors, such as kaolin and quartz, with the aim to formulate consolidating solutions using natural materials and design specific restoration mortars compatible with the substrates to be restored [28].

2.2 High temperature resistant binders and matrices for fiber reinforced composites

Calcium hydroxide can represent a dangerous trigger point for degradation process to arise for cementitious binders. High $Ca(OH)_2$ contents, indeed, may significantly affect these binder's stability at high temperatures and in the event of fire, as calcium hydroxide (portlandite) starts to decompose around 450-550°C, thus causing relevant strength reductions, increase of porosity and permeability and, hence, increasing the structure vulnerability to external aggressive attacks. Geopolymers, compared to traditional inorganic binders, besides having comparable or even higher mechanical strength, generally have also a longer life due to their chemical inertness and their higher thermal resistance, because of the absence of water and hydrated or organic compounds in their structure. Depending on their initial composition, they can resist to temperatures up to 1200°C, as they do not burn, ignite or release toxic smoke even after a prolonged exposure: in case of fire or high-temperature exposure they usually syntherize, merge or expand [29]. Low-calcium alkali-activated systems, in facts, because of the absence or a negligible content of portlandite among the reaction

products, generally show a higher thermal stability: this means that alkali-activated binders can provide an attractive technological alternative to traditional cements in applications where stability at high temperatures is required, as for example refractory materials or fire protective coatings.

These outstanding features brought scientific research to investigate the feasibility of replacing organic polymers with alkali activated binders in composite materials design. As regards structural applications for building engineering, a commonly used repair method for damaged concrete and masonry structures consists in the application of fiber reinforced polymers (FRP), in most cases in the form of woven fiber fabrics applied on site by means of epoxy resins. As the fire resistance of any building structure mainly depends on the thermal properties of its constituent materials, the weak high-temperature behaviour and flammability of these organic materials may significantly limit their use. Inorganic alkali-activated binders can instead provide excellent high thermal stability, as well as good adherence and compatibility with most of the building materials because of the chemical interaction between the alumino-silicate that constitute both the substrate and the coating materials. Mineral and polymeric fibers were successfully used to cast geopolymer composites for structural rehabilitation [30, 31], both in the form of unidirectional continuous fiber sheets and bidirectional mesh grids, or in the form of short dispersed chopped fibers. Contrarily to organic resins, according to the densification and crystallization process that the geopolymer matrix undergo upon heating, the mechanical properties of the composites can be further improved: unidirectional carbon fiber reinforced geopolymers were found to exhibit higher values for flexural strength, work of fracture and Young's modulus when exposed to a temperature range of 1100 to 1300°C [32].

2.3 Steel reinforced mortars and concretes

In traditional OPC concretes, one of the main causes that brings to a premature consistent loss of efficiency for steel reinforced structures and affect their durability is represented by steel bars corrosion. Therefore, it is very important to find out if alternative binders can effectively act as proper cement substitutes in steel reinforced concrete elements and structures. Few research works have been carried on to investigate the behaviour of an alkali-activated binder in presence of steel reinforcements and its ability to effectively passivate the rebars. It has been found that the use of soluble silicates as inhibitor of the corrosion of steel can be as efficient as using chromate-based inhibitors, because of the formation of an insoluble iron silicate, which acted as a barrier for further corrosion [33], or the formation of an iron aluminate amorphous product from the reaction of aluminate anions with the surface of the steel. Alkali-activated silico-aluminates are hence believed to exhibit a high adhesive strength on steel elements and act as a protective layer to prevent corrosion. The stability of the formed protective film mainly depends on the used alkaline activators, but the lower permeability of the binders formulated from sodium silicate and sodium hydroxide has been found to substantially retard the carbonation process, thus ensuring a longer life to the protective film in standard conditions [29]. Some studies have already demonstrated that alkali-activated fly ash mortars can passivate reinforcing steel as rapidly and effectively as Portland cement mortars in standard chloride contents environments [34] and the bond characteristics of reinforcing bar in a geopolymer concrete have been found to be comparable or superior to Portland cement concrete [35, 36]. The mechanical properties and durability performances that geopolymers and alkali-

activated reinforced concretes can offer suggest that using these innovative inorganic binders may result a viable option for reducing the environmental impact and achieve promising results in structural applications.

3 Experimental

3.1 Background and experimental program

Accordingly with previous considerations, the aim of the first part of this work is thus to define a sustainable traditional lime-based organic-inorganic matrix that may be suitable to pre-impregnate and bond carbon fibre fabrics to masonry or natural stone substrates, preserving the original nature of the reinforced materials, without adding any incompatible cementitious material or other organic compounds. In rehabilitation of historical architecture, in facts, externally bonded carbon fibre reinforced polymers have been considered a very efficient solution, due to their proved stiffness and load bearing capacity increase. By now, a wide range of ancient buildings and structures have been strengthened and reinforced using such systems, especially in seismic areas, where a rapid and easy repairing intervention is required [37-40]. Despite the various advantages that fiber reinforced polymers (FRP) systems can exhibit, such as light weight and high corrosion resistance, some structural problems, up to complete failure, can arise. One of these major drawbacks could be substantially identified with composite's matrices and bonding materials, which must ensure adhesion among reinforcing elements and substrate surfaces [41-46]. The effectiveness of such repairing technique is indeed

mainly affected by bond properties and adhesion between the fibers and substrate. Conventional FRP systems are based on thermosetting organic resins, which usually are not applicable on wet surfaces and are substantially non-reversible. Furthermore, their behaviour is heavily UV and temperature dependent, so generating several problems that might be overcome to grant better results [47]. Other relevant issues contributing to define the reinforcing system's global efficiency may be remarked. In the last decades an increasing attention has been focused to low-impact technologies for both environmental and human health preservation. It is therefore noteworthy that these conventional epoxy-based techniques could not be considered completely hazard free for workers' health and environment, and a serious need to find valid alternatives, able to grant comparable results in terms of mechanical properties, is pointed out [47-51]. Moreover, in rehabilitation of existing earthquake-damaged structures, fiber reinforced polymer systems are necessarily related to ease and quickness of application, minimizing installation time and avoiding two-component bonding systems, that might create serious problems with *in situ* dosage and mixing procedure, as well as slow-curing epoxy systems.

A possible solution to overcome these problems is hence here investigated: epoxy-based adhesive was replaced with a sustainable organic-inorganic binding matrix, based on traditional lime putty. The final goal is hence to obtain carbon fiber reinforced pre-impregnated fabrics able to minimize inconsistency with historical architectural substrates, maintain the required flexibility in structural rehabilitations, improving adhesion and speed up the application procedures.

In the second part of this research work, with the aim to go on with the research on low impact inorganic matrices, fiber reinforced composite materials based on geopolymers

were then investigated. As already said, geopolymers are in facts representing one of the most promising green and eco-friendly alternative to OPC binders in different applications fields, including that of engineered fiber reinforced composites for structural repair interventions [30, 47, 51-54]. However, the poor tensile and bending strengths usually exhibited by geopolymers, given their brittle and ceramic-like nature, can easily lead to catastrophic failures and represents the main drawback limiting the use of those materials in several applications. Fiber reinforced geopolymer composites may be considered a solution to improve flexural strength and fracture toughness of these materials, thus enabling their use in architectural rehabilitation. Different types of fiber reinforcements have already been employed in various geopolymer systems to improve their flexural strength, impact behaviour and failure mode [30, 51-54]. It has been reported that adding reinforcing fibers to a brittle matrix helps to control micro and macro-cracks diffusion through the material by generating a bridging effect [51, 53-58], as well as to change the post-cracking behaviour of the material from a brittle fracture mode to a ductile one, thanks to its enhanced strain energy dissipation ability [54-60]. In this study different types of short fibers were thus embedded in an alkali-activated inorganic matrix. High Tenacity (HT) carbon, E-glass, polyvinyl alcohol (PVA) and polyvinyl chloride (PVC) fibers were chosen and several tests have been carried out in order to determine the adhesion of each type of fiber to the matrix and their ability to improve the geopolymer's flexural strength and toughness.

Alkali-activated materials are usually synthesized at temperatures between 20 and 80 °C from metakaolin or industrial wastes such as coal fly ash and blast furnace slag which have already been using successfully in several industrial applications [10, 61-64].

With the aim to further reduce the use of non-renewable raw materials and increase the

use of un-exploited industrial by-products, research has recently been concerned with the alkali activation of ladle slag [65]. Ladle slag is a by-product of the steelmaking industry that uses electric arc furnaces. Ladle slag represents about one third of the total amount of slag usually produced in an electric arc furnace and European production is estimated to be about 4 million tonnes a year [66]. Compared to blast furnace slag, ladle slag is richer in calcium oxide and poorer in silica content [67]. The use of a calcium-rich raw material, such as ladle slag, as a precursor for alkali-activated material production has great potential for the building industry: it has been previously demonstrated that systems based on ladle slag and metakaolin are able to form, by alkali activation, calcium-rich alumino-silicate gels with impressive mechanical properties [65].

Many studies have already been conducted on the influence of varying concentrations of calcium in the starting materials have on hydration and hardening processes on the final properties of alkali-activated materials (AAM). Alkali-activated materials synthesized from low and high-calcium fly ash have been widely investigated [17, 18, 68-70]. It has been observed that small amounts of Ca (4-8 wt. %) can improve compressive strength, as well as enabling room temperature setting. For greater amounts of Ca, calcium silicate hydrates phases (C-S-H) have been identified as coexisting with the alumino-silicate phase, formed in alkali activated materials [17, 71, 72]. The C-S-H phases exist in ordinary Portland cement (OPC) and are the significant contributors to mechanical strength formation.

Alkali activated blast furnace slag based binders can exhibit similar or better properties than OPC systems in terms of strength, reduced shrinkage and higher chemical durability, as reported in previous research [18-20, 73]. Alkali-activated materials

including Ca have other properties that make them attractive for use as novel materials for civil engineering. For instance it has been reported that the high temperature behaviour of these materials is superior to their OPC equivalent [18-20, 73, 74]. Dombrowski et al. [17] found that 8 wt. % of calcium hydroxide in alkali-activated fly ash based mixtures lead to better performance at high temperature, compared with calcium free alkali-activated materials.

Accordingly, this research aims to investigate the high-temperature behaviour and the relevant effects on the compressive strength of Ca-rich alkali activated materials based on ladle slag with the goal to develop fully sustainable materials made by from different waste streams. As a starting point, metakaolin/ladle slag mixes have been alkali activated and the products evaluated. The metakaolin/ladle slag products have been compared with coal fly ash/ladle slag products to ascertain the suitability of replacing metakaolin with fly ash as alumino-silicate source material. The joint activation of ladle slag and other alumino-silicate raw materials (metakaolin or fly ash) has been hence proposed as an effective approach to develop sustainable materials based on industrial waste.

Finally, in order to assess the effective viability of using alkali-activated materials as new sustainable binders in building and construction engineering, other important properties have been hence evaluated. A successful industrial adoption of geopolymers and alkali-activated materials requires indeed that they can be easily coupled with commonly used rebars to cast steel reinforced concrete and mortars and show good durability properties. Chloride and other soluble salts transportation into inorganic binders is critical from the viewpoint of protection of reinforcements, as it has been widely demonstrated for OPC based mortars. Presumably, given their high alkalinity, even

higher than in traditional mortars, alkali-activated mortars will guarantee negligible levels reinforcement corrosion and of chlorides diffusion, thus ensuring sufficient durability properties and comparable or even higher corrosion resistance.

In this context, the effective ability of an alkali-activated mortar to protect an embedded steel reinforcing element against corrosion has been considered: corrosion resistance has been evaluated by means of induced corrosion tests and obtained results have been analyzed and correlated with each sample's microstructure. The protecting behaviour of alkali-activated mortars has hence been compared to that of OPC based mortar, to highlight any remarkable difference between ordinary and new-designed binding systems based on the joint activation of waste materials as ladle slag and fly ash.

3.2 Materials

3.2.1 Lime-based prepreg carbon fabrics for architectural rehabilitation

To formulate the pre-impregnating and binding matrices for the fiber reinforced composite, a 3 moths aged lime putty [LG] (Calceviva Candor), from Adriatica Legnami S.r.l (Fasano (BR) Italy) was alternatively used. Water-dispersible vinyl-acetate terpolymer [VA] (Vinavil S.p.A., Milano, Italy) was chosen to additivate the obtained inorganic matrices. A cementitious binding matrix, used as comparison basis, was mixed with cement CEM II/A-LL 42,5R [C] from Italcementi (Calusco d'Adda (BG) Italy). Unidirectional HT-carbon fiber fabrics [CF] (Betontex, Casalecchio di Reno, BO, Italy), with a tensile strength of 4800 MPa and a density of 320 g/m, were

used to prepare all the reinforcing sheets. Prismatic clay bricks of 5,5 x 5,5 x 25 cm (fornace Sant'Anselmo, Loreggia, Padova, Italia) were used as substrate elements for all the reinforcing CF sheets.

3.2.2 High-toughness fiber reinforced alkali-activated matrices

Alkali-activated matrices were prepared from blends of ladle slag and metakaolin powders. Ca-rich ladle slag was supplied by Rubiera steel plant located in Casalgrande (RE, Italy): a first sieving treatment was necessary to obtain a grain size distribution <63 μm before mixing, thus retaining only an 88% of the slag (Fig. 1a). The resulting ladle slag powder [LS], with an average particle size of 28 μm, was then blended with metakaolin to cast different batches of samples. Metakaolin [MK1] was obtained by calcination of a commercial kaolin (Argirec B24, AGS Mineraux, Clerac, France) at 700°C for 5h. Chemical composition for LS and MK1 has been determined by X-Ray Fluorescence Spectrometry on a dry sample basis (loss on Ignition has been determined gravimetrically between 105 and 1000°C): the main oxides composition for LS and MK1 is listed in Table 1. Grain size distribution curves of LS and MK1, determined by a laser particle-size analyzer (Master Sizer 2000, Malvern Instruments), are reported in Fig. 2. XRD diffraction data were also collected for LS and reported in Fig. 3. LS was found to be a mainly crystalline material, having dicalcium silicate (calcio-olivine, γ-C_2S) as the main phase. Other calcium-magnesium-aluminium silicates phases, such as larnite (β-C_2S), mayenite $Ca_2(Al,Fe)_2O_5$ and gehlenite were detected. Low amounts of quartz, calcite ($CaCO_3$) and periclase (MgO) were also evident in X-ray spectra. $CaCO_3$ content in LS has also been calculated by means of a Dietrich-Fruhling apparatus and a

mean value of 6.85% was found. Sodium silicate solution, with a SiO_2:Na_2O ratio of 1.99 (supplied by Ingessil, Montorio, VR, Italy) and 8M NaOH solution were used as alkaline activators. HT-carbon fibers (average fiber diameter: 10 μm, tensile strength: 5490 MPa) were supplied by Torayca-Toray Industries, Tokyo, Japan; commercial E-Glass fibers (average fiber diameter: 10 μm, tensile strength: 2500 MPa) were supplied by Betontex, Casalecchio di Reno, BO, Italy; PVA fibers (average fiber diameter: 18 μm, tensile strength: 1800 MPa) were supplied by Thermofibers S.r.l, Lanzo, TO, Italy and PVC fibers (average fiber diameter: 400 μm, tensile strength: 215 MPa) were supplied by Fili&Forme, S. Cesario sul Panaro, MO, Italy.

3.2.3 High-temperature resistant alkali-activated binders and steel reinforced mortars

Alkali-activated pastes for high-temperature analysis were prepared from blends of ladle slag and metakaolin or ladle slag and fly ash powders. Metakaolin [MK2] was of a commercial type, purchased from Imerys (UK) under the brand name of Metastar 402, with a particle size distribution of 100% < 10 μm. Class F-fly ash [FA], with an average particle size of 8,6 μm, was obtained from Port Augusta power station located in South Australia (Fig. 1b). Grain size distribution of FA was determined by a laser particle-size analyzer (Master Sizer 2000, Malvern Instruments): data are summarized in Fig. 2. Chemical composition for FA has been determined by X-Ray Fluorescence Spectrometry on a dry sample basis (loss on Ignition has been determined gravimetrically between 105 and 1000°C); oxide composition MK2 was obtained from technical data sheets. FA mineralogical composition was determined by XRD and results are reported in fig. 4: its composition is predominantly determined by amorphous

alumino-silicates, with presence of crystalline phases of quartz (20%) and mullite (27%), besides some amorphous iron, hematite, rutile and maghemite impurities (3,5%). Data for ladle slag [LS] have been previously reported and all chemical compositions are summarized in Table 1.

Table 1: Bulk composition (wt. %) and loss on ignition of LS, FA and MK1,2

Oxide composition	SiO_2	Al_2O_3	Fe_2O_3	CaO	MgO	Others	LOI (1000°C)
LS	17.9	13.0	7.1	42.1	6.1	3,8	10.0
MK1	47.6	37.7	8.7	0.1	0.0	5.9	n.d.
MK2	54.8	40.4	0.8	0.1	0.4	3,5	n.d.
FA	52.0	30.5	2.8	4.6	2.5	7,1	0.5

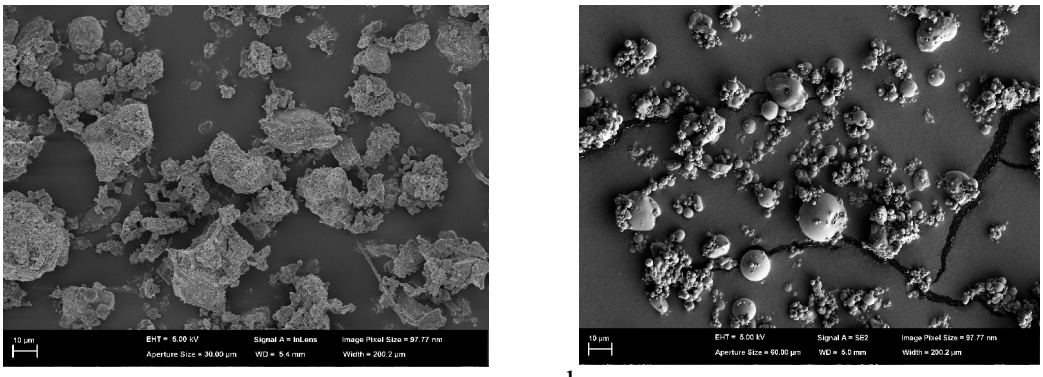

a b

Fig. 1: Ladle slag (a) and Port Augusta fly ash (b) particles (SEM image)

Cab-o-sil untreated fumed silica from Cabot Corp [Cab], with a specific surface area of 200 m^2/g and an average particle (aggregate) length of 0.2-0.3 μm, was also used to adjust the formulations and obtain the desired Si/Al ratios. As alkaline activators, a NaOH 8M solution and a sodium silicate solution, containing 14.7% of Na_2O and 29.4% of SiO_2 (Vitrosol D-A53, PQ Australia), were used.

Alkali activated steel reinforced mortars were prepared from normalized quartz sand and blends of LS and FA, whose details have already been given above. As steel

reinforcement, FeB42K bars with a 6 mm diameter were used.

To cast the reference cementitious mortar samples, a CEM II/A-LL 42,5R [C] from Italcementi (Italcementi, Calusco d'Adda (BG) Italy) was used.

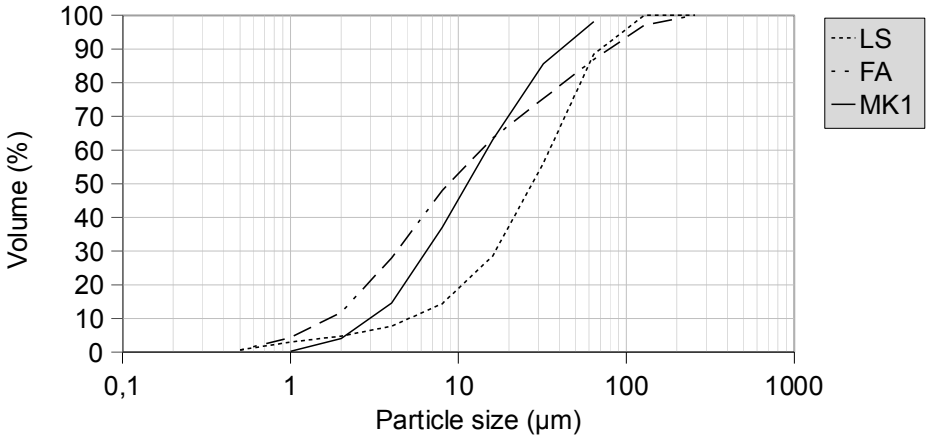

Fig. 2: Grain size distribution for LS, MK1 and FA

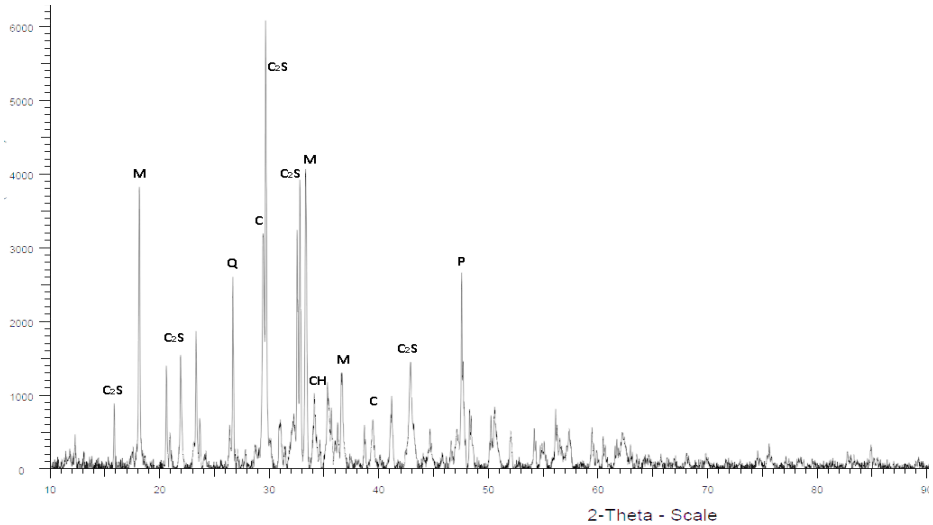

Fig. 3: XRD pattern for LS.
Key: C_2S= γ-Calcium Disilicate (Ca_2SiO_4), M= Mayenite $Ca_2(Al,Fe)_2O_5$, Q= Quartz (SiO_2), C= Calcite ($CaCO_3$), CH= Portlandite $Ca(OH)_2$, P= Periclase (MgO)

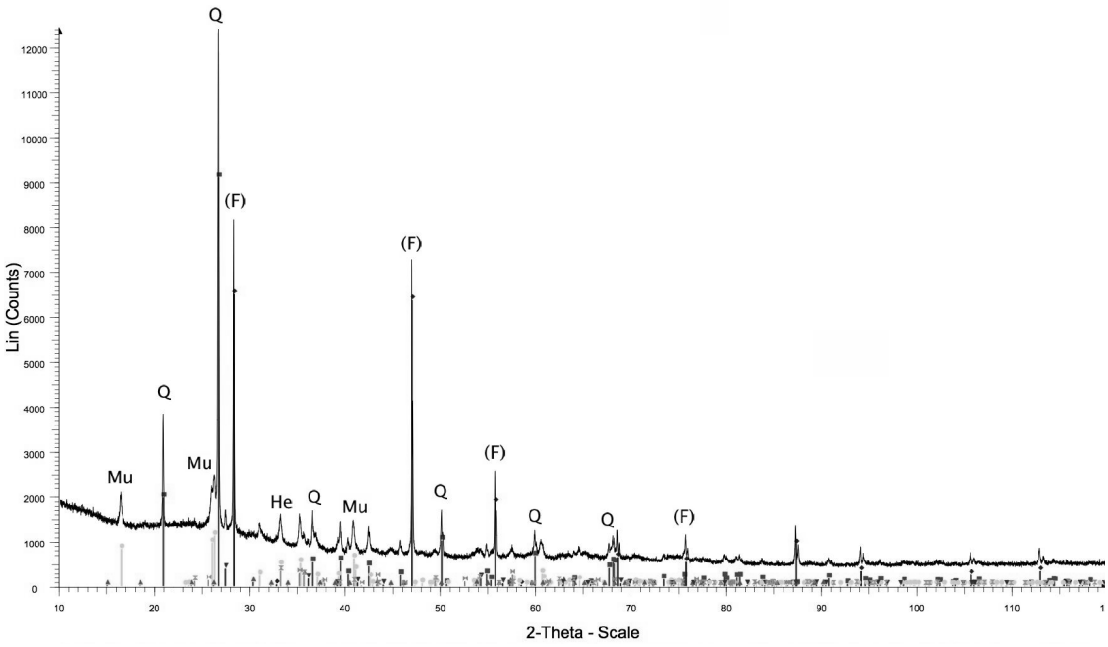

Fig. 4: XRD pattern for FA.
Key: Q= Quartz SiO_2, (F)= Fluorite (CaF_2) – internal standard, Mu= Mullite ($Al_{4.52}Si_{1.48}O_{9.74}$), He= Hematite ($Fe_2O_3$)

3.3 Samples preparation

3.3.1 Lime-based prepreg carbon fiber fabrics

Organic-inorganic matrices were appositely formulated to pre-impregnate the reinforcing carbon fiber fabrics to be applied on the bricks' surface. All carbon fiber sheets were manually cut to fit the clay bricks' width, on which they have been applied as a reinforcing system. A shorter length than the whole bricks' one was then appositely obtained for all the fiber sheets, in order to avoid undesired secondary effects on the end-sides of the specimens while testing. It was previously noticed that when performing bending tests, reinforcing sheets applied on the whole surface of the brick samples might condition specimens' flexural behaviour, thus returning unreliable results.

Pre-impregnation lime-based grouts were obtained by mixing together 2-parts of water-dispersible vinyl-acetate [VA] and 1-part of hydraulic lime putty [LG], without adding any extra water content: the mixture workability, indeed, was good enough to ensure a good penetration between the fiber filaments of the sheets. Correspondingly, as a comparison basis, a pre-impregnation cement-based grout was formulated mixing 2-parts of water-dispersible vinyl-acetate and 1-part of cement [C]. The lime-based binding matrix, used to fix the reinforcing sheets to the substrates, was formulated mixing 2-parts of lime putty with 1-part of vinyl acetate. Similarly, the cement-based one was obtained mixing 2-parts of cement, 1-part of water and 1-part of vinyl acetate. All mentioned formulations are summarized in Table 2.

All prismatic clay bricks were appositely prepared prior to fiber sheets application:

macroscopic flaws were removed from the upper surface by manually sanding and then an air gun was used to eliminate superficial dust and residual clay powder (Fig. 5a). Performing such mechanical treatments on the specimens' surfaces prior to reinforcements' application is proven to play a fundamental role in enhancing adhesion between the substrate and the reinforcing materials [45]. A neat, more irregular and rough surface, indeed, is able to determine the best conditions to ensure adequate mechanical interlock at the interface among reinforcing and reinforced elements.

Table 2: Composition of pre-impregnating and binding grouts for carbon fiber fabrics

Samples	Pre-impregnation grout [parts]				Binding matrix [parts]			
	VA	LG	C	extra H_2O	VA	LG	C	extra H_2O
RG 70/30	2	1	0	0	1	2	0	0
RG NR	0	0	0	0	1	2	0	0
RC 70/30	2	0	1	0	1	0	2	1
RC NR	0	0	0	0	1	0	2	1

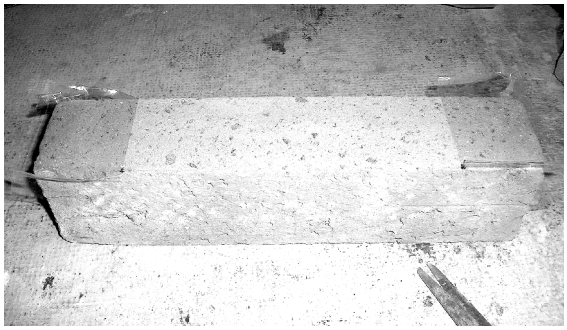

Fig. 5a: Surface treatment on a clay brick specimen prior to fiber application

Fig. 5b: Reinforcing woven fabrics applied on upper bricks' surface

A batch of 8 specimens was then prepared pre-impregnating the fiber sheets on both sides with either the cement or the lime-based grout by hand lay-up technique (RG

70/30 and RC 70/30 for the lime-based and cement-based grout, respectively). The pre-impregnated sheets were then let to cure in laboratory ambient conditions (T=20°C, RH=50%) for 7 days (Fig. 5b). In order to assess the effectiveness of pre-impregnation technique, a second batch of 8 un-impregnated carbon fiber fabrics (4 for each matrix formulation) was also predisposed to be applied on clay brick elements without any previous treatment on the fibers, using either the lime-based or the cement-based binding matrix (RG NR and RC NR for the lime-based and cement-based matrix, respectively). After curing, the pre-impregnated and un-impregnated fiber sheets were applied onto the upper face of the brick elements, using the appositely formulated binding matrices, as reported in Tab.2. A ceramic roll was used to allow a better penetration of the matrix and ensure an adequate bonding between the fiber sheets and the substrate by hand pressing onto the reinforced surface. All reinforced brick specimens, together with plain unreinforced ones, acting as reference samples [REF], were kept in the same laboratory conditions for 2 days before testing.

3.3.2 High-toughness fiber reinforced alkali-activated matrices

The geopolymer composite samples were prepared by adding the reinforcing fiber fraction to a properly designed alkali-activated matrix during the mixing operations, in order to obtain a slurry as homogeneous as possible and grant an adequate dispersion of the fibers within the matrix. The mix design for all the geopolymer samples is reported in Table 3. A reference sample [MK40LS60] was firstly prepared by combining in a planetary mixer both LS and MK1, in a ratio of 3:2 respectively [65] and mixing for 5 min. The alkaline solutions were blended together and then added to the previously

mixed solid fraction, up to obtain homogeneous and workable slurry. No further water additions, that would have been detrimental to mechanical properties [65], were necessary to achieve the adequate workability (Tab. 2).

Table 3: Reference and fiber-reinforced geopolymer samples mix design

Samples	MK1 [g]	LS [g]	NaOH [g]	Na_2SiO_3 [g]	Fiber type	Fiber amount [wt. %]
MK40LS60	140	210	105	105	-	0
Fc-MK40LS60	140	210	105	105	Carbon HT	1
Fg-MK40LS60	140	210	105	105	E-Glass	1
Fpva-MK40LS60	140	210	105	105	PVA	1
Fpvc-MK40LS60	140	210	105	105	PVC	1

The four different fiber types, appositely selected, were cut to obtain a 7±1 mm length and used to prepare fiber-reinforced geopolymers, named as follows Ftype-MK40LS60 (e.g. Fpvc-MK40LS60 means a geopolymer matrix reinforced by PVC fibers). Regardless the fiber type, the same amount of fiber (1% wt. fraction on the total mixture) was added to MK1 and LS in the above reported ratio, then the slurry was mixed for 5 min. Specimens were cast in prismatic moulds of 2x2x12 cm and cured in a humid atmosphere (RH > 90%) at room temperature (20°C) for 7 days.

3.3.3 High-temperature resistant alkali-activated binders

Geopolymer samples were prepared from different formulations, obtained by varying LS and FA amounts or LS and MK2. Two different groups of mixtures were hence conceived: a first group was defined using blends of LS and FA, while a second group, as a comparison basis, was then prepared substituting FA with MK2. In all the

investigated mixtures CaO content was assumed to derive exclusively from LS, the water content was fixed in the range of 23-38% and Na/Al ratio was fixed equal to 1.0. For LS/FA ash group, low calcium [LLSFA] and high calcium [HLSFA] series, with an average CaO content around 5-6% and 18-20% respectively, were taken into account. For LS/MK group, only low calcium series was prepared [LLSMK]. Indeed, it was not possible to obtain LS/MK2 group with high calcium content, as the mixtures were not workable in the mentioned operating conditions.

Table 4: Formulations of the investigated samples

Samples	LS [wt %]	FA [wt %]	MK2 [wt %]	NaOH [wt %]	Na_2SiO_3 [wt %]	Cab [wt %]
LLSMK 2.0	12.7	-	31.8	5.8	49.6	0.0
LLSMK 2.5	8.9	-	29.9	10.0	41.4	8.9
LLSMK 3.0	10.0	-	25.1	0.0	47.5	10.8
LLSFA 2.0	14.8	52.9	-	22.8	9.5	0.0
LLSFA 2.5	16.4	48.7	-	9.2	25.6	0.0
LLSFA 3.0	12.8	49.7	-	7.7	26.8	3.1
HLSFA 2.0	49.1	15.0	-	13.9	22.1	0.0
HLSFA 2.5	46.9	15.1	-	4.5	32.4	1.1
HLSFA 3.0	41.5	17.5	-	0.4	37.1	3.3

Table 5: Si/Al, Na/Al ratios, CaO and total water content of the investigated mixtures

Samples	Si/Al [wt%]	Na/Al [wt%]	CaO [wt%]	H_2O [wt%]
LLSMK 2.0	2.0	1.0	5.3	32.3
LLSMK 2.5	2.5	1.0	5.3	32.5
LLSMK 3.0	3.0	1.0	5.2	38.0
LLSFA 2.0	2.0	1.0	6.2	23.8
LLSFA 2.5	2.5	1.0	6.8	25.2
LLSFA 3.0	3.0	1.0	5.3	24.3
HLSFA 2.0	2.0	1.0	20.6	23.5
HLSFA 2.5	2.5	1.0	19.7	24.7
HLSFA 3.0	3.0	1.0	17.5	23.5

To investigate the combined effect of different amounts of Ca, Si and Al in the geopolymerization process, three different Si/Al ratios of 2.0, 2.5 and 3.0 for each of the above mentioned batches were also taken into account. Accordingly, samples were named with the relative acronym followed by 2.0, 2.5 or 3.0, depending on their specific Si/Al ratio (e.g. LLSFA 2.0 stand for low-Ca ladle slag/fly ash mixture, Si/Al = 2.0). The starting materials were hence mixed for 5 min in a planetary mixer, and 6 samples for each formulation were cast by pouring the slurry into 25 ml polypropylene cylindrical moulds sealed with a polyethylene screw lid. All samples were de-moulded after 24 hours curing in humid atmosphere and then cured in a humid tank at ambient temperature with a relative humidity >90% for 7 days. Smaller samples for dilatometry measurements were appositely cast into 5 mm diameter plastic cylinders and cured in the same conditions. Once de-moulded, the cylinders were cut to obtain a 15 mm length. The investigated mixtures are summarized in Table 4 and 5.

3.3.4 Alkali-activated steel reinforced mortars

Alkali-activated steel reinforced mortars were prepared from LS/FA mixtures in order to perform corrosion resistance and durability tests. Two distinct LS and FA mix formulations were prepared by diversifying the LS content: a low-calcium series, with a CaO content of 6.2%, and a high-calcium series, with a CaO content of 20.6% were designed. Both low-Ca and high-Ca mixtures were formulated with a specific Si/Al ratio of 2.0 and Na/Al of 1.0, while water content was set equal to 23.8 and 23.5% for low-Ca and high-Ca respectively. The alkali activated mortars were hence prepared from these formulations by Hobart mixer, with binder and normalized quartz sand

mixed in a weight ratio of 1 to 2.7. Water and liquid alkaline solutions were added in different proportions, to obtain the desired Si/Al ratio and workability.

A reference batch of samples was also obtained by preparing a standard OPC mortar, according to the normalized mix-design reported in UNI-EN 196-1.

All mix formulations are summarized in Tab. 6. Mortar samples were named as follow: M-, followed by LLSFA 2.0- and HLSFA 2.0- for the low-calcium and high-calcium samples respectively. Reference cementitious samples were named as M-CEMII-. Each sample name was then followed by a number, indicating the curing time (e.g. M-LLSFA 2.0-21 refers to a low-calcium mortar obtained with MK and FA and cured for 21 days, M-CEMII-7 refers to a OPC-based mortar cured for 7 days).

Prismatic specimens (160x40x40 mm) were hence prepared to perform flexural and compressive strength tests.

Table 6: Formulations of the investigated mortars

Samples	LS [g]	FA [g]	C [g]	NaOH [g]	Na_2SiO_3 [g]	Sand [g]	H_2O [g]
M-LLSFA2.0	119	423	-	182	76	1350	0
M-HLSFA2.0	393	120	-	111	176	1350	0
M-CEMII	-	-	450	-	-	1350	225

Cylindrical samples (h= 100 mm, d= 45 mm) with a 140 mm length reinforcing steel bar centrally embedded (Fig. 6) were then cast for corrosion resistance measurements. Before moulding the reinforced mortars, the steel bars were cleaned with a wire brush and coated for 80 mm with an anticorrosion epoxy coating (Top-Armatec 108, Sika). The steel bars were hence sunk in the fresh mortars, leaving a coated legth of 20 mm deep inside the sample, in order to avoid crevice corrosion at the top surface of the

cylinders. The samples were cured in a humid tank (RH> 90%) at 20°C for the first 24 h and then demoulded. They were successively left to cure in the same humid conditions for different curing times, from 7 to 21 or 28 days. Before testing, samples' bottom surface was coated with a 2-5 mm thick paraffin layer, to prevent ions diffusion process coming from the bottom of the samples.

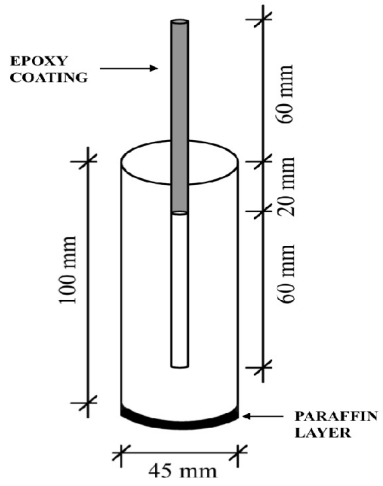

Fig. 6: Reinforced mortar sample's preparation

3.4 Samples characterization

3.4.1 Mechanical properties

Flexural strength of unreinforced clay bricks and bricks externally bonded with pre-impregnated and un-impregnated carbon fiber fabrics (REF, RC 70/30 and RG 70/30, RC NR and RG NR respectively) was determined by three point bending test setting a span of 17 cm for all tested specimens. Mechanical properties were determined as

average value on at least three samples by an Amsler–Wolpert machine with a constant strain rate of 50 mm/min. Moreover, to evaluate the adhesion strength of the reinforcing system and the maximum tensile load (perpendicular to the reinforced specimens' surface) that the reinforcement can bear before detaching from the support, a pull-out test was arranged, according to ASTM D 4541-02, by an adhesion tester Elcometer 106.

Short fiber reinforced and unreinforced geopolymer matrices (Ftype- MK40LS60 and MK40LS60 respectively) were tested with a three-point bending technique as well, setting a span of 8 cm for all tested specimens. As for these samples, load-deflection curves were also recorded, in order to determine their energy absorption capability by defining flexural toughness indices and residual strength factors, according to ASTM C1018-97. Load bearing increase was determined for all fiber reinforced samples by comparison with respective reference unreinforced samples. A direct examination of the flexural behaviour and fracture type was also performed. The amount of energy absorbed during fracture and ductility of reinforced geopolymer specimens was also determined by Charpy impact strength tests on 2x2x4 cm samples. A Zwick Charpy pendulum, equipped with a 15 J hammer, was used. All impact strength tests were conducted on batches of at least 3 samples and reported results are an average value of 3 tests.

Compressive strength for LLSFA, HLSFA and LLSMK alkali-activated materials was determined using an Instron-5500R testing machine with a strain rate of 5 mm/min until 2 kN then 7422 N/min. The uncertainty in the measurement was taken as the standard deviation of the compressive strength of at least 3 samples.

Compressive and flexural strength tests for M-LLSFA, M-HLSFA and M-CEMII mortar samples were performed with an Amsler–Wolpert machine with a constant strain rate of

50 mm/min. Measures were conducted on at least 3 samples and average values were reported.

3.4.2 Optical microscopy

As for pre-impregnated carbon fiber fabrics (RC 70/30 and RG 70/30), to assess the degree of penetration of the lime-based matrix among carbon fibers filaments and any possible difference in coated sheets surfaces, an optical microscopy (Wild 3M Heerbrugg stereoscope) was used.

3.4.3 Microstructural characterization

Microstructure observations were performed on fracture surfaces of fiber reinforced Ftype- MK40LS60 geopolymers by a Philips XL20 scanning electron microscope (SEM) and phase recognition of the investigated geopolymer matrix samples was acquired by energy dispersive X-ray (EDX 9800 microanalysis).

The amount of calcium carbonate ($CaCO_3$) in LLSFA, HLSFA and LLSMK geopolymers was calculated with a Dietrich-Fruhling apparatus by reacting 1 g of dried grinded sample with 10% HCl in a sealed reaction cell. SEM images for these samples were taken with a Zeiss Neon 40EsB focused ion beam scanning electron microscope on epoxy-coated polished samples and XRD patterns were collected on a D8 Advance diffractometer (Bruker AXS, Germany) from 5˚ to 80˚ 2Θ (step size 0.02˚ 2Θ and speed 0.4°/min).

Pore size distribution measurements for all samples (Ftype- MK40LS60, LLSFA, HLSFA, LLSMK, M-LLSFA, M-HLSFA and M-CEMII) were carried out by a mercury intrusion porosimeter (MIP, Carlo Erba 2000) equipped with a macropore unit (Model 120, Fison Instruments).

3.4.4 Thermal analysis

To evaluate thermal resistance of LLSFA, HLSFA and LLSMK geopolymer samples and the influence of high-temperatures on micro-structural, physical and mechanical properties, all specimens have been calcined up to 1000°C, in an electric furnace with a heating rate of 2 °C/min and cooled down to ambient temperature by a progressive temperature decrease. Samples characterizations, including mechanical tests, have hence been performed on untreated and calcined samples. To evaluate geopolymers' dimensional stability upon heating, dilatometry tests have also been conducted, according to ASTM E831-9, with a Adamel Lhomargy DI-24 dilatometer by exposing the samples over a temperature range of 20–1000°C (heating rate: 5°C/min). A preload of 65 mN was set to allow the instrument to record data from shrinking samples.

3.4.5 Corrosion tests and durability analysis

Corrosion resistance of geopolymer or cementitious (as a reference basis) reinforced mortars (M-LLSFA, M-HLSFA and M-CEMII) was evaluated by means of electrochemical tests performed at different curing times. Accelerated corrosion tests have been performed by Impressed Voltage (IV) technique: samples were dipped into a

3.5% NaCl solution, surrounded by a galvanized steel cage (Fig. 7).

Steel bar (working electrode, WE), galvanized steel cage (counter electrode, CE) and $Hg/HgCl_2$ electrode (saturated calomel electrode, SCE, as reference, RE) were connected (3-electrode system) to a potenziostat (Potenziostat 7050 Amel Instrument). A constant voltage of 5 V was applied by the external potenziostat between the reinforcement (anode) and galvanized steel cage (cathode) with 3.5% NaCl solution working as electrolyte. IV tests have been carried on for 6 days on each sample and anodic current activity have been recorded as a function of time.

At the end of IV test, linear polarization resistance technique (LPR) was then used to evaluate steel corrosion current intensity.

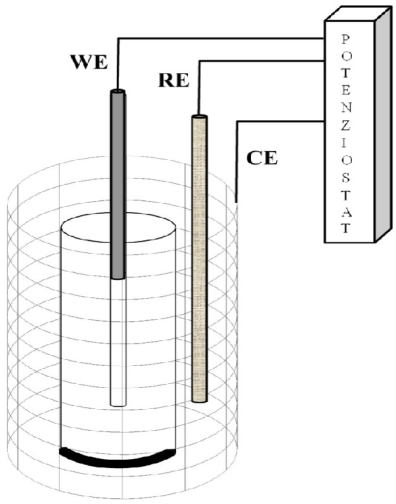

Fig. 7: Impressed voltage test set-up

pH was also determined on powdered mortar fragments obtained by cylinder specimens after IV and LPR tests. About 8.00 g of ground mortar (100% passing at 0.106 mm sieve) were stirred for 2 h with 250 ml of boiling water, and then filtered: the solution was titrated by AgNO3 0.1 N (potassium bichromate as indicator) and pH was measured by a 315i WTW digital pHmeter. The content of water-soluble chlorides was determined

by mortar samples grinding, salts extraction with distilled boiling water, filtration and ion chromatography performed with an IC Dionex ICS 1000.

4 Results and discussion

4.1 Lime-based prepreg carbon fabrics for architectural rehabilitation

4.1.1 Flexural strength enhancement and fracture behaviour

Flexural resistance and adhesion tests on strengthened clay bricks have been carried out: accordingly with results obtained for polymer-added cementitious matrices, a significant enhancement of the load-bearing capacity of the specimens reinforced with lime-bonded carbon fabrics has been achieved. Flexural strength values [R_f], flexural strength increments relative to unreinforced clay bricks [ΔR_f] and fracture types for all specimens are reported in Tab.7.

All reinforced samples exhibited an improvement in their flexural behaviour, returning an average strength increment of about 65%, referring to unreinforced reference samples. These results can thus confirm that all the designed reinforcing systems, based on organic-inorganic sustainable matrices, can enhance significantly the flexural load bearing capacity of a fragile substrate material such as clay bricks.

Almost all tested samples failed by crushing of the support in the compressed region

of the specimens, thus indicating that reinforcements have worked properly. Delamination of the reinforcing sheets only occurred for RG 70/30 sample, probably due to an incomplete penetration of the binding matrix between the fiber filaments: the partially setting of the pre-impregnation layer of the carbon fiber sheet, prior to its application, could have prevented the fibers to get well impregnated by the matrix. In most cases, instead, fiber filaments were found to be bonded to the substrate material, even after failure (Fig. 8), so that a generally improvement in system ductility was achieved.

Table 7: Flexural strength and fracture type of reinforced and unreinforced clay bricks. Key: D= Crisis for delamination of the reinforcement from the support; K= Crushing compression of the support; S= Shear crisis of the support

Samples	Rf [MPa]	Δ Rf [%]	Fracture Type
REF	6.7	-	-
RG 70/30	10.7	+59	D
RG NR	11.2	+66	K
RC 70/30	12.5	+85	K
RC NR	10.3	+53	K

Table 8: Pull-off strength of reinforced clay bricks.
Key: C= Cohesive fracture (in the substrate material); A= Adhesive fracture (along the interface between adhesive and reinforcing materials); M= Mixed fracture (among the reinforcing fibers)

Samples	R_P [MPa]	Fracture type
RG 70/30	1.0	A
RG NR	1.0	C
RC 70/30	3.0	M
RC NR	1.5	C

Regarding flexural strength data, no significant differences were noticed between lime-based and cement-based systems. Both pre-impregnated and un-impregnated lime-based samples (RG 70/30 and RG NR, respectively) showed good results, thus indicating that a more compatible and non-invasive lime-based strengthening system can grant adequate flexural strength enhancement, just as a cement-based one. A slightly higher value was recorded for RC 70/30 sample, and it is likely that the water content in the binding matrix could have contributed to hydrate the un-hydrated cement particles of the pre-impregnation cementitious layer, thus generating a stronger bond between the fiber sheet and the substrate.

4.1.2 Adhesion properties and pull-off strength

The adhesion properties of the designed matrix and its ability to adequately penetrate and impregnate the reinforcing fiber sheets were firstly analyzed. Optical microscopy images taken on pre-impregnated RC 70/30 and RG 70/30 woven fabrics after a 2 days curing time are reported below (Fig. 8 a, b).

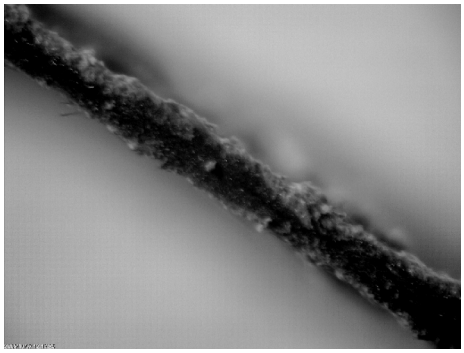

Fig. 8 a: Cross-section of pre-impregnated RC 70/30 woven fabric
(16X)

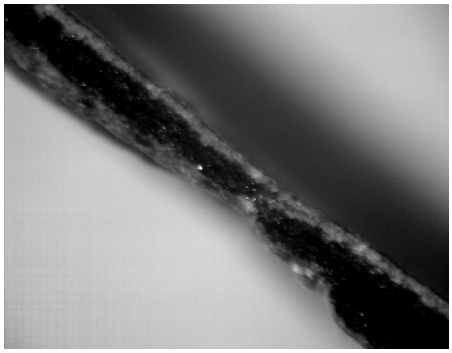

Fig. 8 b: Cross-section of pre-impregnated RG 70/30 woven fabric
(16X)

For both RC 70/30 and RG 70/30 pre-preg specimens, the upper plain surface resulted almost regular, with no evident flaws or detachments of the applied matrix from the fibers, thus meaning that a proper impregnation of the reinforcements was achieved. As it can be clearly seen from the reported images, indeed, both the lime-based and the cement-based pre-impregnating matrices adhered to the carbon fibers. However, a slightly higher degree of penetration and a thicker covering layer was

detected on fiber sheet pre-impregnated with the cementitious matrix (RC 70/30). Good adhesion properties between the substrate material and the reinforcing elements characterized all the tested specimens, even though some differences could be pointed out, depending on whether or not a pre-impregnation layer was covering the fiber sheets or whether the binding matrix was a cement-based or a lime-based one.

Pull-off test results, accordingly to ASTM D 7522 and CNR 200-2004, are reported in Table 8. Although the preferable fracture type for strengthening and reinforcing systems (cohesive) has been observed only for the untreated bonded fabrics (both with cement based and lime-based matrix, RC NR and RG NR (Fig. 9 a), respectively), a positive fracture behaviour characterized also the prepreg cement and lime-bonded samples. The highest pull-off strength value was indeed registered for the cement pre-impregnated sample (RC 70/30), even though it exhibited a mixed fracture type (Fig. 9 b). This system, indeed, was found to collapse for a fracture generated in the pre-impregnating layer, probably the weakest part of the whole system, but without any deferential effect on his final behaviour. Here, in facts, the loose bonded fibers were pulled-out from the matrix quite slowly: that instance surely contributed to reach higher strength values and allow the system to exhibit a

more ductile, and thus preferable, fracture behaviour.

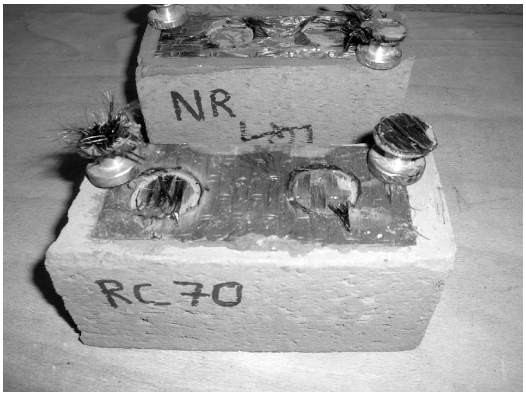

Fig. 9 a: Pull-out test on reinforced (RC NR and RC 70/30) brick samples.

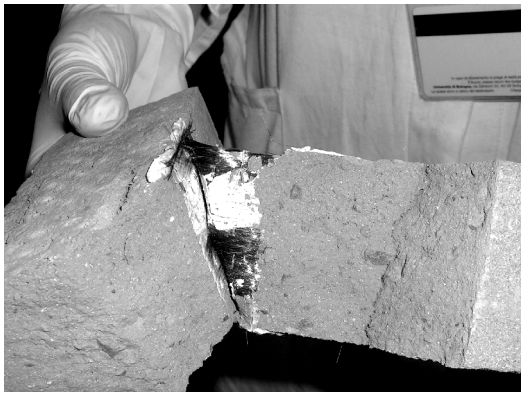

Fig. 9 b: Mixed fracture type for RC 70/30: fiber filaments still bonded to the substrate after failure are visible.

Woven carbon fabrics that have not been preimpregnated, neither with a cement or lime-based matrix (RC NR and RG NR), exhibited the most desirable cohesive fracture type, but with lower values of pull-off strength. It can thus be deduced that a better adhesion between the reinforcing system and clay bricks' surfaces can be achieved if no pre-treatments on the fibers are applied, but the achieved strength at the interface layer between the fibers and the binding matrix might be weaker. A cohesive fracture behaviour hence indicates that a proper mechanical interlock between the binding matrix and the substrate was achieved, but in these cases a fewer percentage of the reinforcing fibers suffered a favourable pull-out effect upon fracture, thus resulting in a less ductile behaviour.

As for the lime-based systems, compared to the cementitious one, no macroscopic differences were found, thus demonstrating that sustainable lime-based binding systems can be as successful as the cementitious ones. Only a slight decrement for the pull-off strength was found, probably due to the weaker nature of the natural

binder compared to OPC. However, similar flexural strength increments were found, referring to unreinforced samples, and favourable fracture types, together with a pull-out mechanism of the embedded fibers from the matrix, were detected.

4.2 High-toughness fiber reinforced alkali-activated matrices

4.2.1 Mechanical and physical properties

Several tests have been carried out on fiber reinforced geopolymer samples (Ftype-MK40LS60) in order to determine the adhesion of each type of fiber to the matrix and their ability to improve the geopolymer's flexural strength and toughness. Results from mechanical and microstructure characterization of all obtained geopolymer composites are here reported and discussed.

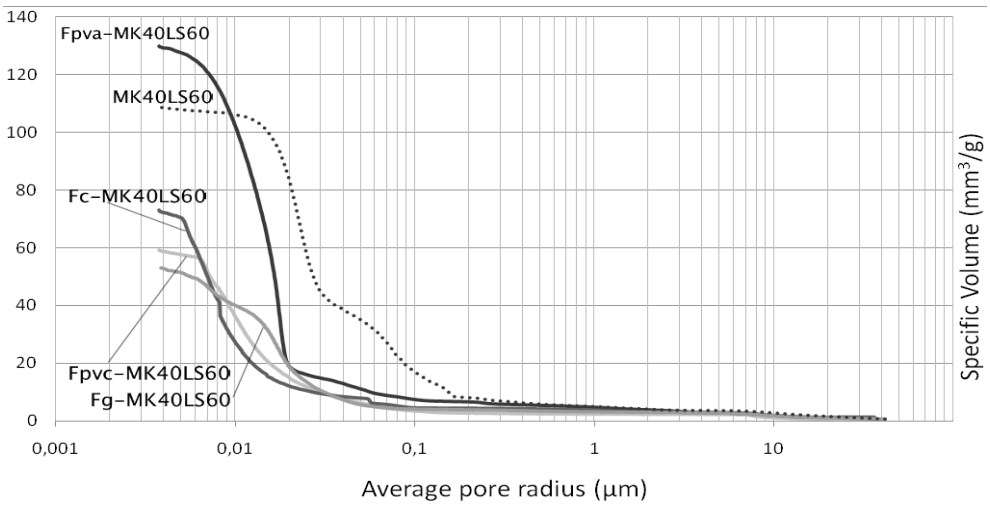

Fig. 10: Pore size distribution for geopolymer composite samples

Pore size distributions for fiber-reinforced and unreinforced (dashed line) geopolymer samples are reported in Fig. 10. Reported data (Tab. 9) show clearly that the addition of reinforcing fibers generally resulted in a reduction of the intruded volume, except for Fpva-MK40LS60: specific intruded volume for the investigated

samples lies in the range of 52.5-129.1 mm^3/g, where the highest values were recorded for the reference sample (MK40LS60) and PVA reinforced sample (Fpva-MK40LS60).

A remarkable difference in the pore network distribution between carbon, glass and PVC reinforced samples and the reference one could be pointed out, the latter showing a more homogeneous and uniform distribution. The pore network for the unreinforced sample, in fact, comprises a system of mesopores from 20 to 200 nm that was not observed in the fiber-reinforced specimens, whose pore distribution is mainly defined by smaller pores (4-20 nm) (Fig. 10). Nevertheless, despite the reduction of the intruded volume found in most reinforced samples, their average pore radius (R_{av}) was found to be slightly higher after the addition of fibers (Tab. 9), especially for glass and PVA reinforced samples.

Table 9: Physical and mechanical properties of geopolymer composite samples

Samples	Specific intruded volume [mm^3/g]	R_{av} [µm]	R_f [MPa]	ΔR_f [%]
MK40LS60	108.3	0.006	6.9	-
Fc-MK40LS60	72.2	0.009	11.7	+ 70
Fg-MK40LS60	52.5	0.016	9.0	+ 30
Fpva-MK40LS60	129.1	0.016	11.2	+ 62
Fpvc-MK40LS60	58.5	0.009	10.0	+ 45

Besides increasing average pore radius, fiber addition had a direct effect on mechanical properties. Flexural strength (Rf) indeed strongly increased for all fiber-reinforced samples, whose strength increments (ΔR_f) ranged between 30-70% if compared to unreinforced geopolymer. Maximum values were found for carbon fiber

reinforced sample (Fc-MK40LS60) (Tab. 9). Increased mechanical strength for fiber-reinforced samples resulted in accordance with the lower total porosity values and the bridging effect adduced by the dispersed fibers. Even Fpva-MK40LS60, whose total porosity was found higher than the reference sample's one, exhibited a clear flexural strength gain. This is likely to be due to the stronger crack-bridging behavior of PVA fibers due to a high-grade adhesion to the geopolymer matrix and, thus to a more efficient load transfer mechanism.

4.2.2 Flexural toughness and residual strength

Flexural toughness and post-cracking ductility of fiber-reinforced samples were also investigated. Load-deflection curves for geopolymer composites, along with unreinforced control samples (MK40LS60) were determined (Fig. 11). As shown in Fig. 10, post-cracking behaviour is significantly improved by fiber addition. Reinforcing fibers are clearly contributing to extend the area under the non-linear portion of the load-deflection curve and, thus, to enhance the energy absorbed by the material during fracture.

All added fibers were able to determine for the reinforced geopolymers a change from a plain linear behaviour (MK40LS60), where the energy absorption capacity just concerns the simultaneous onset of fracture and initiation of cracking, to a typical ductile behaviour, where the energy absorption is mainly determined by micro-cracks growth and propagation and progressive fiber debonding up to failure [55].

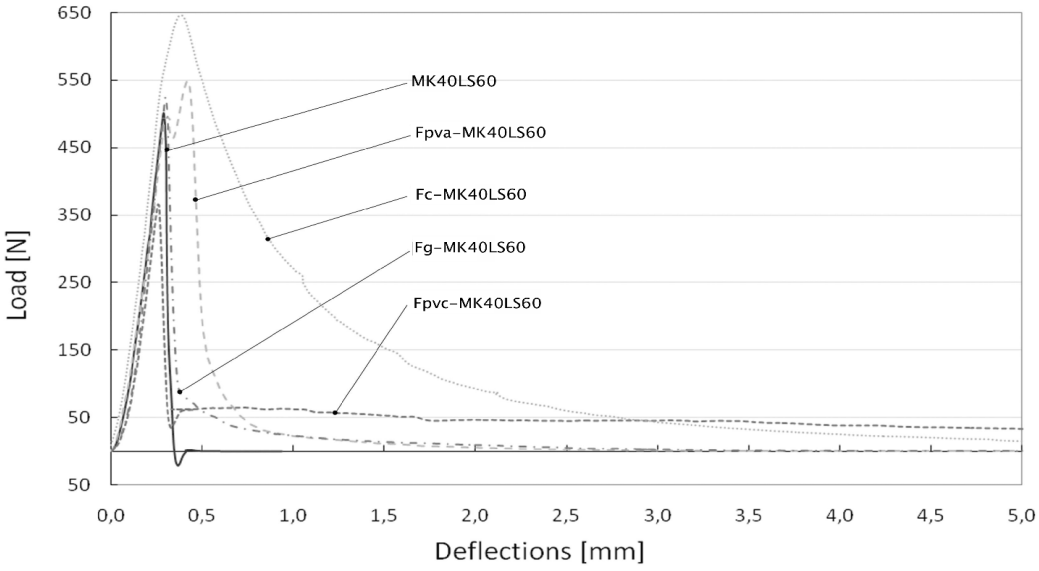

Fig. 11: Load-deflection curves for all geopolymer composite samples

Table 10: Toughness and residual strength of geopolymer composite samples

Samples	Resilience* [J/cm^2]	Toughness Indices			Residual Strength Factor	
		I_5	I_{10}	I_{20}	$R_{5,10}$	$R_{10,20}$
MK40LS60	2.2	1.0	1.0	0	0.00	0.00
Fc-MK40LS60	3.1	4.6	6.5	8	38.62	14.41
Fg-MK40LS60	2.2	1.7	1.9	2.0	4.51	1.55
Fpva-MK40LS60	2.6	3.1	3.4	3.5	4.67	0.86
Fpvc-MK40LS60	2.4	2.0	3.2	4.9	22.47	17.30

Moreover, the energy absorption capacity is significantly influenced by the type of reinforcing fibers used in the mixtures: carbon and PVC fibers showed higher fracture toughness and ductility, as it can be seen from the wider curve branch that describe the composites' behaviour after reaching the first-crack load. These fibers were demonstrated to have a better bridging behaviour within the cracked matrix as they were able to induce a favourable pull-out mechanism that occurred when fracture arose.

To quantify the fracture energy content of the fiber-reinforced geopolymers, toughness indices and residual strength factors were determined according to ASTM C1018-97 (Tab. 10) [60]. The closer I_5, I_{10} and I_{20} are to values of 5, 10 and 20 respectively, the more the material's behaviour can be approximated to perfectly plastic after first crack. Carbon fiber-reinforced sample Fc-MK40LS60 shows the best response after first crack load, providing the higher values for all toughness indices and residual strength factor $R_{5,10}$. The latter represents the average level of strength retained after first crack as a percentage of the first-crack strength.

4.2.3 Microstructural characterization and fiber adhesion

Microstructure investigations were performed on cured samples by SEM-EDS to point out gels structure and composition (Fig. 12), as well as fiber-matrix interface (Fig. 13). It can be noticed that the geopolymerization process successfully occurred and all investigated samples exhibited a mainly amorphous structure (Fig. 12, 13). EDX investigations evidence the formation of C-A-S-H gels generated by geo-synthesis for all the samples, although in each sample differences in microstructure were observed. A more homogeneous and close-grained structure was found to be related to higher values of Si/Al ratios in the geopolymer matrix (detected Si/Al values ranged from 1.1 to 3.7).

Investigated samples showed that both organic (Fig. 11a) and inorganic (Fig. 11b) fibers are able to sufficiently adhere to the geopolymer matrix. However, polymer fibers seem more efficient in controlling and preventing the micro-cracks propagation (Fig. 11).

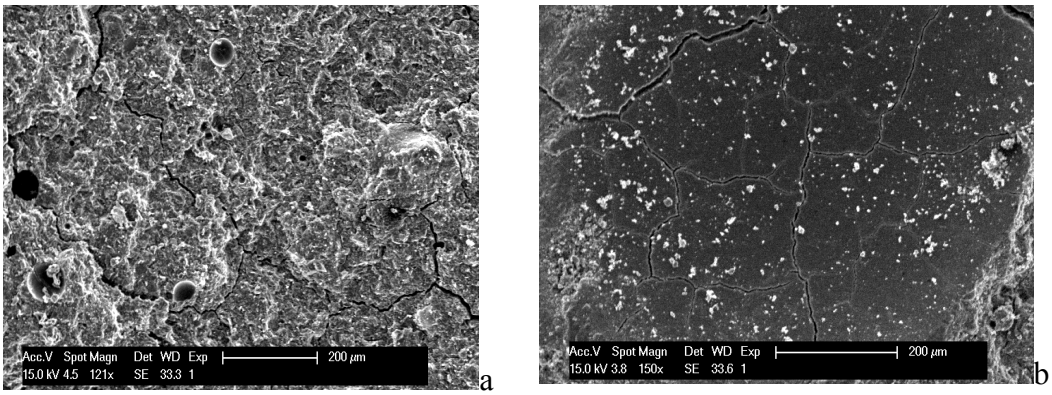

Fig. 12: (a) SEM observation for MK40LS60 sample, 120 X; (b) SEM observation for MK40LS60 sample, 150 X

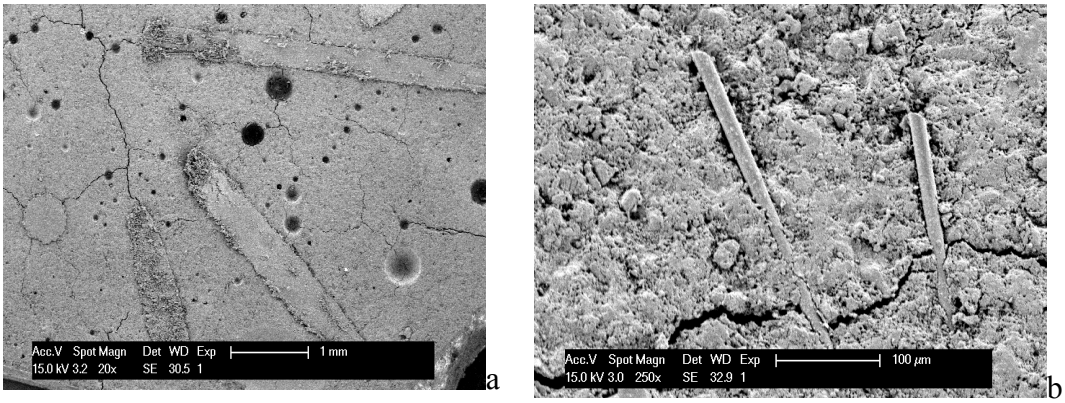

Fig. 13: (a) SEM observation for Fpvc-MK40LS60 sample, 20 X; (b) SEM observation for Fg-MK40LS60 sample, 250 X

In particular, PVC fibers were observed to have the best adhesion properties, probably due to their sensibly higher diameter. The strong bond between these fibers and the matrix, however, did not make the pull-out more difficult and, thus, did not affect the toughness of the material significantly.

4.3 High-temperature resistant alkali-activated binders

4.3.1 Microstructural characterization

XRD analysis was conducted on LLSMK, LLSFA and HLSFA samples in order to determine the extent of activation and the phase composition of the main reaction products.

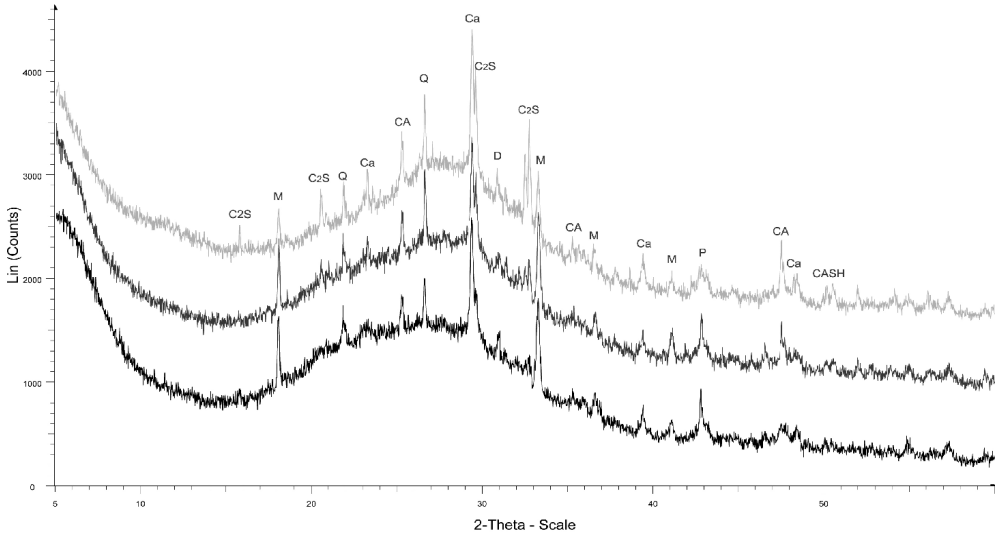

Fig. 14: XRD patterns for LLSMK. From the top: LLSMK 2.0, LLSMK 2.5 and LLSMK 3.0.

Key: Q= Quartz, Ca= Calcite, P= Periclase, C_2S= γ-Calcium Disilicate (Ca_2SiO_4), CA= Calcium Aluminum Oxide ($Ca_3(Al_2O_6)$), M= Mayenite ($Ca_{12}Al_{14}O_{33}$), D= Dolomite $MgCa(CO_3)_2$, CASH= Gismondine ($CaAl_2Si_2O_8 \cdot 4H_2O$)

For metakaolin based samples (Fig. 14) the crystalline phases detected after alkali-activation are mainly calcium based and as such derive from the ladle slag precursor. The dominant crystalline phases were calcium silicate (γ-C_2S (01-087-1257)), calcium aluminium oxide (00-033-0251) and calcium carbonate (01-072-1937)

phases. Mayenite (00-048-1882), dolomite (04-008-0789), periclase (00-045-0946) and quartz (03-065-0466) were also detected.

There was evidence of a C-A-S-H phase ($CaAl_2Si_2O_8 \cdot 4H_2O$), besides some other unidentified amorphous phases as noted by a significant broad diffraction hump at 20-35 2θ (Fig 14). The intensity of the crystalline peaks in the XRD patterns are believed to be related to the Si/Al ratio of the sample: the intensity of the diffraction peaks corresponding to the γ-C_2S phase was observed to decrease as the silicate concentration increased from Si/Al 2.0 to 3.0 (Fig. 14).

Table 11: $CaCO_3$ content of cured samples

Samples	$CaCO_3$ [wt. (bulk sample mass)%]	$CaCO_3$ [wt.(tot. $CaCO_3$) %] (relative amount created by geopolymerization)
LS powder	6.9	-
LLSMK 2.0	10.0	91.3
LLSMK 2.5	5.8	89.5
LLSMK 3.0	4.2	83.8
LLSFA 2.0	7.9	87.1
LLSFA 2.5	7.8	85.6
LLSFA 3.0	6.7	86.9
HLSFA 2.0	18.9	82.2
HLSFA 2.5	11.0	70.7
HLSFA 3.0	13.0	78.2

The presence of $CaCO_3$ in LLSMK samples was also found to decrease with increasing Si/Al ratio, moving from 10.0 wt. % for LLSMS 2.0 to 4.2 wt.% for LLSMK 3.0. Ladle slag contains 6.9 wt. % of $CaCO_3$, suggesting that the alkali

activation has increased the calcite content. Calcite is likely to formed by the carbonation reaction of $Ca(OH)_2$, previously obtained during the activation process (Table 11).

XRD analysis of the fly ash-based samples (Fig. 15) indicated that increasing the CaO content in the mix resulted in changes in the identified crystalline phases. High-calcium based samples (HLSFA) are defined by a wide range of reflections corresponding to γ-C_2S, calcite, mayenite and periclase. Crystalline phases, such as quartz and mullite, from the fly ash precursor were also detected. Low-calcium based mixtures exhibited higher peak intensity for the quartz and mullite phases due to the greater concentration of fly ash in the mixes. Periclase, calcium and magnesium aluminium oxide phases were also detected, being slightly more evident for high-calcium based samples. LLSFA and HLSFA samples did not have a C-A-S-H phase that was detectable by XRD. The reactions involved in the alkali activation process that determine the nature and the amount of dissolved species in the mixtures appear to be conditioned by the Si/Al ratio of the sample. LLSFA samples show no remarkable differences with increasing Si/Al ratio, except for an obvious reduction in γ-C_2S peak intensity. HLSFA samples exhibit a similar sharp decrease in γ-C_2S peaks intensity with increasing Si/ Al ratio as well as a slight reduction of quartz, mayenite and mullite peak intensity. As previously found for LLSMK mixtures, also in fly-ash based samples $CaCO_3$ amount is generally found to be higher for samples with Si/Al= 2.0. In LLSFA calcium carbonate content of 7.9 (± 0.45), 7.8 (± 0.25) and 6.7 (± 0.8) wt.% was found for LLSFA 2.0, 2.5 and 3.0, respectively. HLSFA samples, as expected, showed the highest content of calcium carbonate (18.9 (± 1.05), 11.0 (± 0.70) and 13.0 (± 0.55) for HLSFA 2.0, 2.5 and 3.0, respectively) (Tab. 11).

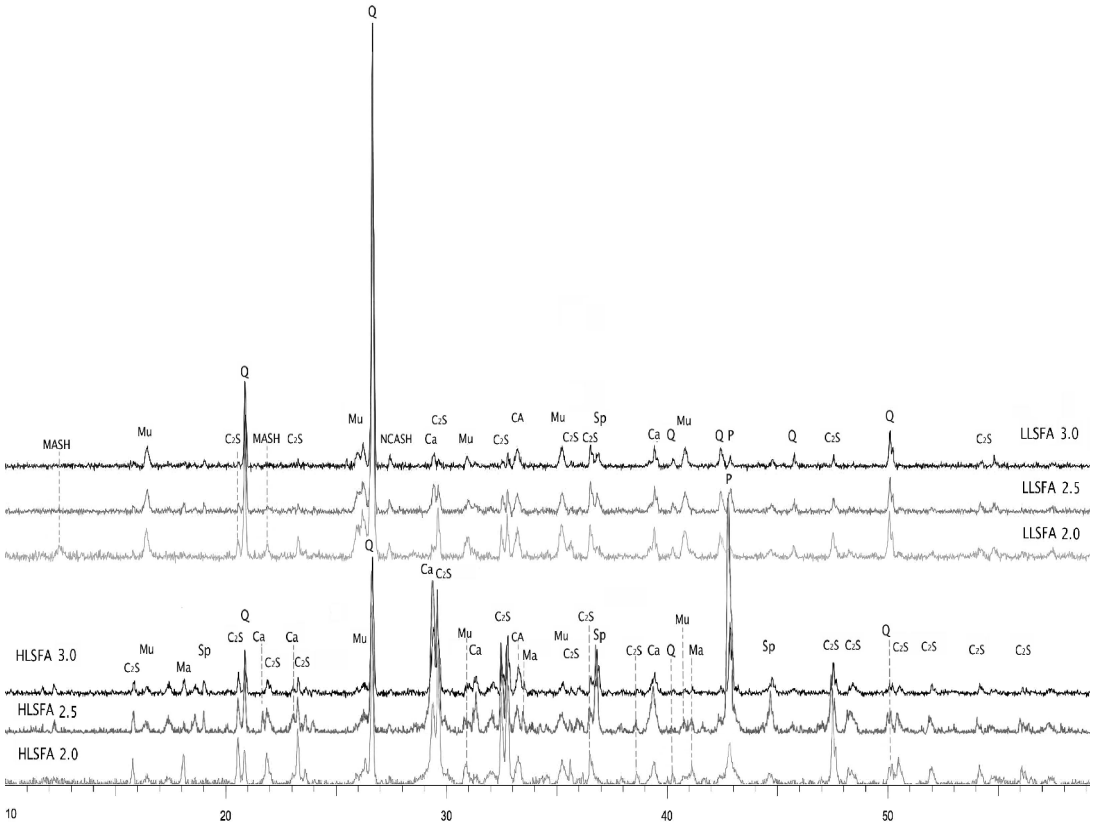

Fig. 15: XRD pattern for LLSFA (top) and HLSFA (bottom) samples. From the top, LLSFA 3.0, LLSFA 2.5, LLSFA 2.0; HLSFA 3.0, HLSFA 2.5, HLSFA 2.0. Background hump has been removed for better clarity.

Key: Q= Quartz, Ca= Calcite, P= Periclase, C_2S= γ-Calcium Disilicate (Ca_2SiO_4), CA= Calcium Aluminum Oxide ($Ca_3(Al_2O_6)$), MASH= Magnesium Aluminum Silicate Hydrate ($Mg_{2.85}Al_{5.7}Si_{10.3}O_{32}\cdot 14H_2O$), NCASH= Cancrinite group ($Na_8Al_6Si_6(CO_3)_{0.3}O_{24}(OH)_{1.4}(H_2O)_6$), Mu= Mullite ($Al_{4.64}Si_{1.36}O_{9.68}$), Sp= Spinel ($MgAl_2O_4$).

4.3.2 Effect of thermal exposure

XRD analysis was performed on the samples after they had been calcined at 1000 °C. The intensity of the amorphous hump was observed to reduce significantly after thermal exposure of the LLSMK samples (Fig. 16) and promote the formation of

new crystalline phases (Fig. 17). Calcining induced the amorphous phase to crystallise to phases such as wollastonite (04-010-2581), nepheline (00-035-0424), sodium anorthite (04-007-9875), calcium aluminum silicate ($Ca_3Al_6Si_2O_{16}$, 00-023-0105) and Na-rich plagioclase feldspar (albite, $Na(Si_3Al)O_8$, 00-010-0393).

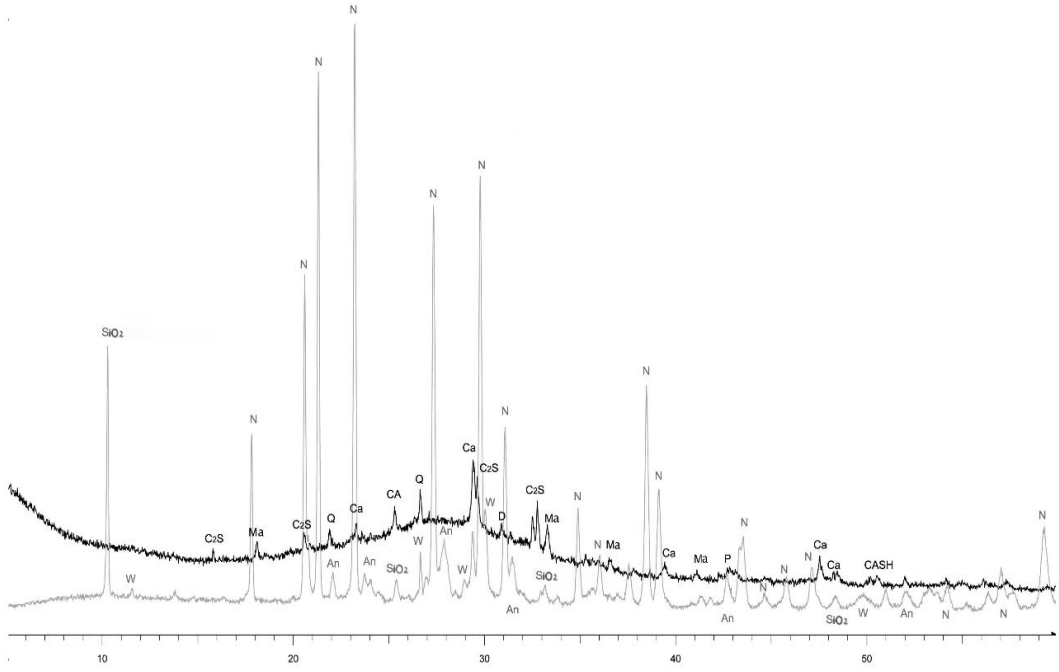

Fig. 16: XRD patterns for untreated (black line) and calcined (gray line) LLSMK 2.0

Key: SiO2= Silicon Oxide (SiO_2), Ca= Calcite, P= Periclase, C_2S= γ-Calcium Disilicate (Ca_2SiO_4), CA= Calcium Aluminum Oxide ($Ca_3(Al_2O_6)$), Ma= Mayenite ($Ca_{12}Al_{14}O_{33}$), D= Dolomite ($MgCa(CO_3)_2$), CASH= Gismondine ($CaAl_2Si_2O_8{\cdot}4H_2O$), An= Na-rich Anorthite ($Ca_{0.8}Na_{0.2}Al_{1.77}Si_{2.23}O_8$), N= Nepheline ($NaAlSiO_4$), W= Wollastonite ($CaSiO_3$)

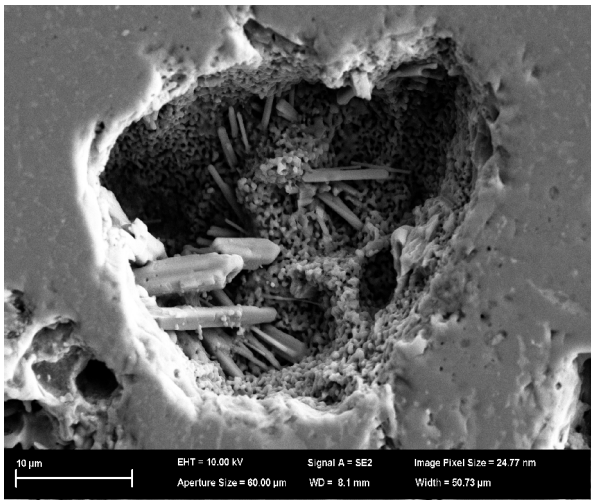

Fig. 17: SEM observation for sample LLSMK 2.0 after calcination, 2000 X

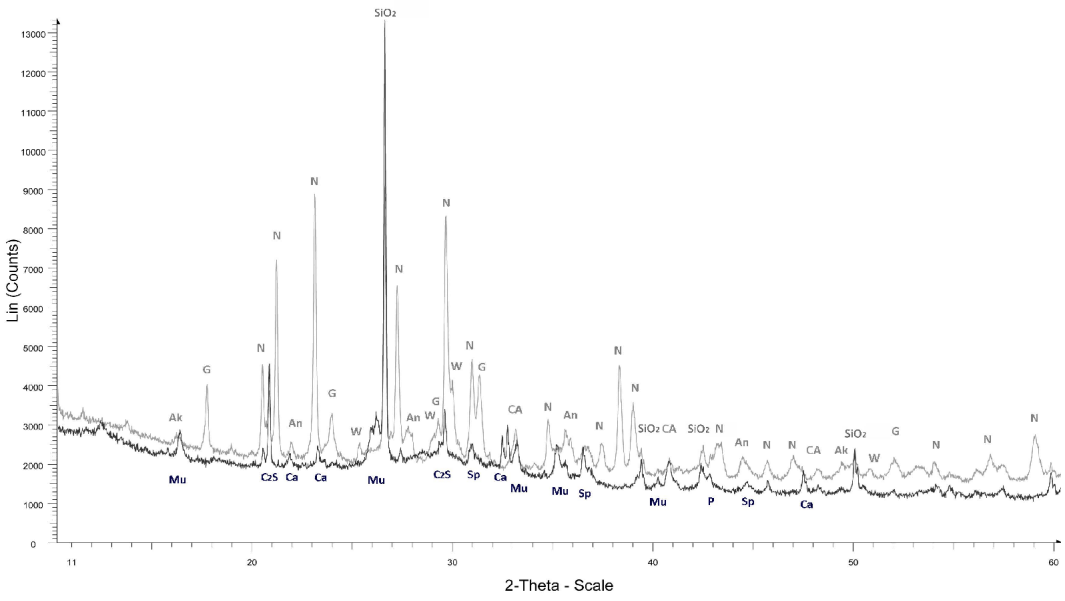

Fig. 18: XRD patterns for untreated (black line) and calcined (gray line) LLSFA 2.0 sample

Key: Q= Quartz, CA= Calcium Aluminium Oxide ($Ca_3(Al_2O_6)$), Ca= Calcite, C_2S= γ-Calcium Disilicate (Ca_2SiO_4), Mu= Mullite ($Al_{4.64}Si_{1.36}O_{9.68}$), Sp= Spinel ($MgAl_2O_4$), P= Periclase, G= Gehlenite magnesian $Ca_2(Mg_{0.25}Al0.75)(Si_{1.25}Al_{0.75}O7)$, Ak= Akermanite, magnesian ($Ca_2(Mg_{0.75}Al_{0.25})(Si_{1.75}Al_{0.25}O_7)$), An= Na-rich Anorthite ($Ca_{0.8}Na_{0.2}Al_{1.77}Si_{2.23}O_8$), N= Nepheline ($NaAlSiO_4$), W= Wollastonite ($CaSiO_3$)

Nepheline starts to form at high temperatures (600°C) from the decomposition of amorphous alumino-silicates and zeolitic phases such as sodalite and is believed to further form Na-rich feldspar (anorthite) if sufficient amounts of calcium and silicon dioxide are still available [17].

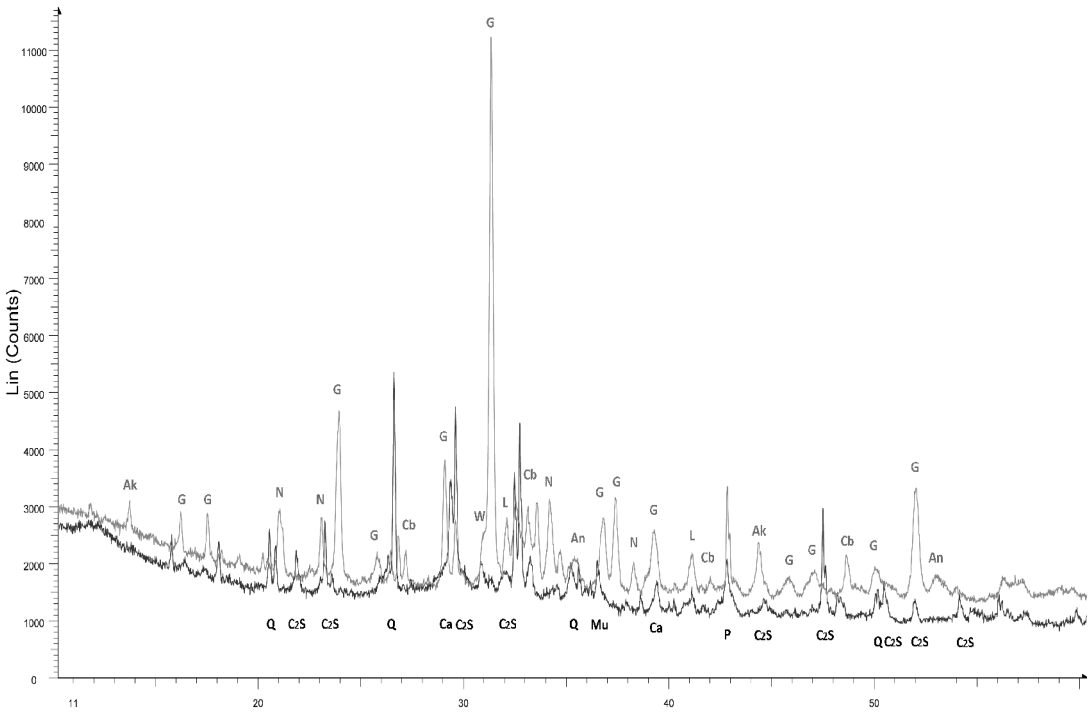

Fig. 19: XRD patterns for untreated (black line) and calcined (gray line) HLSFA 2.0 sample

Key: Q= Quartz, Ca= Calcite, C_2S= γ-Calcium Disilicate (Ca_2SiO_4), Mu= Mullite ($Al_{4.64}Si_{1.36}O_{9.68}$), P= Periclase, G= Gehlenite magnesian $Ca_2(Mg_{0.25}Al_{0.75})(Si_{1.25}Al_{0.75}O_7)$, Ak= Akermanite, magnesian $(Ca_2(Mg_{0.75}Al_{0.25})(Si_{1.75}Al_{0.25}O_7))$, An= Na-rich Anorthite ($Ca_{0.8}Na_{0.2}Al_{1.77}Si_{2.23}O_8$), N= Nepheline ($NaAlSiO_4$), W= Wollastonite ($CaSiO_3$), Cb= Combeite ($Na_6Ca_3Si_6O_{18}$), L= Larnite ($Ca_2SiO_4$)

In LLSFA and HLSFA samples the calcium amount in the original mix strongly influenced the final phase composition of the material after calcination. Thermally induced crystal structures were mainly defined by Ca, Mg silico-aluminates, spinels

and feldspars, depending on the amount of decomposed mineral phases available for re-crystallization. Calcined LLSFA samples (Fig. 18) mainly form nepheline and silicon dioxide, with lower amounts of akermanite, Na-rich anorthite, gehlenite and wollastonite, generated by the re-crystallisation of anhydrous aluminosilicate phases into more thermally stable phases. The calcined HLSFA samples (Fig. 19) had gehlenite ($Ca_2Al_2SiO_7$) as the main phase, as well as wollastonite ($CaSiO_3$) and Na-rich alumino-silicate (nepheline) and calcium-silicate minerals (combeite and anorthite). Therefore, calcination treatment leads to the formation of different phases as a function of calcium content present in the sample. When calcium content is low (LLSMK2.0 and LSFA 2.0) nepheline is the new crystalline phase mainly formed, whilst when calcium amount is high (HLSFA), gehlenite is largely formed. Such behaviour is thought to affect significantly physical and mechanical samples properties.

4.3.3 Thermal behaviour

Thermal expansion/shrinkage results for the samples in this study are presented in Figure 20. All samples were tested after a pre-drying at 105°C to remove the free water to avoid an excessive shrinkage in the initial stage that would prevent contact between the sample and the pushrod of the dilatometer. All LLSMK samples exhibited shrinkage up to 400 °C, (Fig. 20 a) due to the dehydration of weakly bound water from the AAM and the dehydroxylation of chemically bound water. The shrinkage is particularly evident for LLSMK 2.0 sample where dehydration of C-A-S-H phase plays an important role. The C-A-S-H content decreases with the increasing Si/Al ratio as indicated in the XRD analysis.

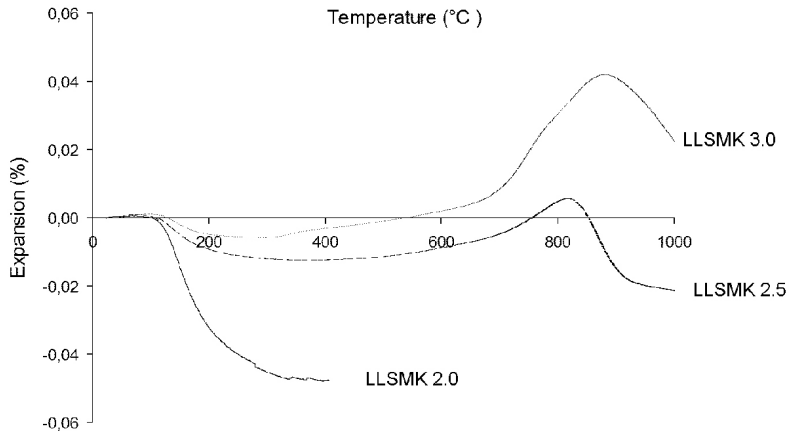

Figure 20 a: Thermal shrinkage versus temperature on LLSMK samples

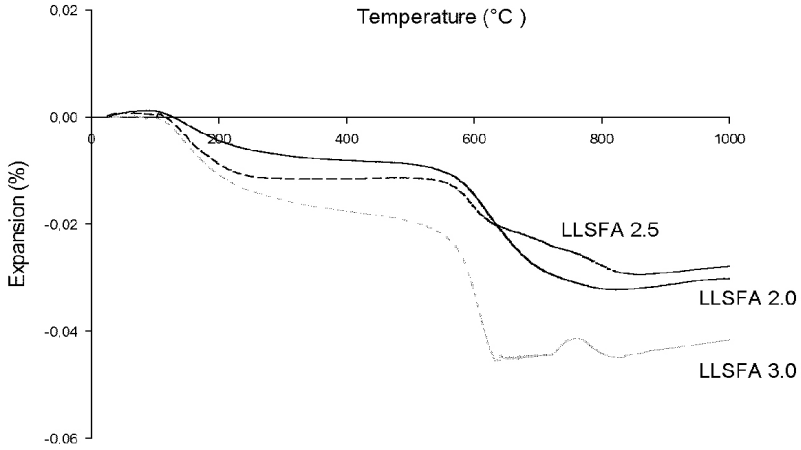

Figure 20 b: Thermal shrinkage versus temperature on LLSFA sample

The thermal behaviour of LLSMK 2.5 and LLSMK 3.0 resembles the curves of geopolymers made from metakaolin as reported by Temuujin et al. [75].

Above 400 °C, the samples expand up to 800 °C, with increased intensity as the Si/Al ratio increases. Beyond 800°C the samples resume shrinking as the sintering process occurring results in the collapse of the pore structure formed during the

previous expansion (Fig. 21). The densification process is confirmed by the measured increase in the apparent density of the calcined LLSMK samples (Tab. 12).

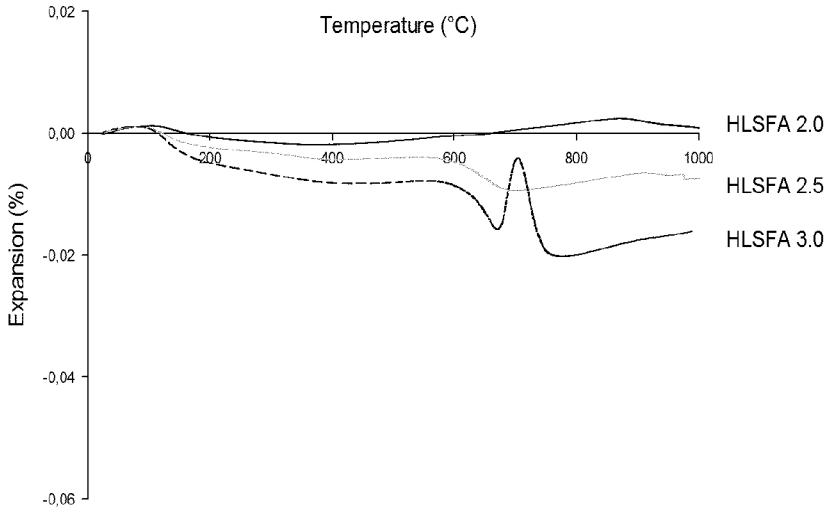

Figure 20 c: Thermal shrinkage versus temperature on HLSFA samples

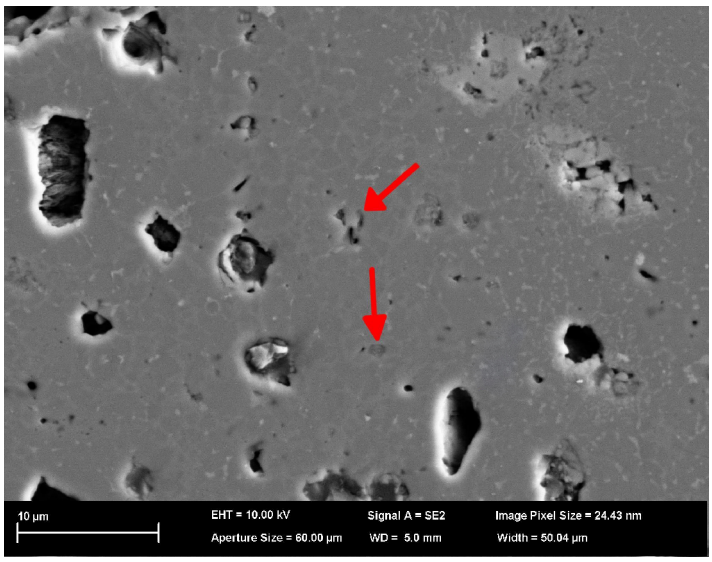

Fig. 21: Sample LLSMK 2.5 after thermal treatment (2000X): collapse of the pore structure are indicated by red arrows

Thermal expansion measurements on LLSFA and HLSFA samples (Fig. 20 b and c) showed different behaviour when compared with the LLSMK samples. LLSFA

sample began shrinking at 150 °C, then after a period of thermal stability up to 600 °C; the samples shrank as sintering occurred.

HLSFA mixes (Fig. 20 c) had greater dimensional stability compared to LLSFA samples (Fig. 20 b) with the same Si/Al ratio. Shrinkage is usually attributed to dehydroxylation process below 300°C and free pore water evaporation [76, 77] (Duxson et al.). However, the introduction of different amounts of ladle slag in fly ash-based geopolymers leads to the formation of different crystalline phases at high temperatures which influences thermal expansion. At high temperatures Ca-rich samples such as the HLSFA samples form Ca-based crystal structures such as gehlenite and wollastonite, which have high melting points (1590°C and 1540°C, respectively) and relatively low values for thermal expansion coefficient ($28.3 \cdot 10^{-6}$ $°C^{-1}$ and $6.5 \cdot 10^{-6}$ $°C^{-1}$ respectively [78, 79]) and, as such, result in a high thermal stability. The lower thermal expansion of these mineral phases, compared to that of nepheline and anorthite ($51.3 \cdot 10^{-6}$ $°C^{-1}$ and $1.53 \cdot 10^{-5}$ $°C^{-1}$ respectively) [80, 81], that mainly define LLSFA samples microstructure after calcination, can thus explain the evidenced better dimensional stability upon heating of HLSFA series.

4.3.4 Mechanical properties

The results from compressive strength testing and density analysis before and after calcination are reported in Table 12.

The relatively low amount of calcium (5.4 wt% of CaO) present in LLSMK mixes resulted in compressive strengths of about 45 MPa with the exception of the Si/Al = 3.0 sample. No remarkable differences in the mechanical properties were observed in LLSMK by increasing the Si/Al ratio from 2.0 to 2.5.

Table 12: Compressive strength and bulk densities before and after thermal exposure

Samples	7-days compressive strength [MPa]	compressive strength after thermal treatment [MPa]	ρ [apparent] [g/cm3]	ρ [apparent] after heating [g/cm3]
LLSMK 2.0	44.2 (8.8)	8.9 (3.4)	1.50 (0.11)	1.72 (0.54)
LLSMK 2.5	46.4 (10.6)	26.3 (1.3)	1.35 (0.23)	1.53 (0.22)
LLSMK 3.0	18.6 (3.5)	4.9 (4.8)	1.68 (0.03)	1.61 (0.06)
LLSFA 2.0	11.0 (3.8)	20.4 (7.5)	1.68 (0.88)	1.60 (0.25)
LLSFA 2.5	12.4 (2.7)	26.4 (0.6)	1.52 (0.24)	1.64 (0.80)
LLSFA 3.0	14.5 (3.2)	41.7 (1.7)	1.58 (0.72)	1.62 (0.66)
HLSFA 2.0	20.6 (3.5)	7.7 (2.6)	1.75 (0.09)	1.72 (0.85)
HLSFA 2.5	13.6 (0.8)	7.8 (0.1)	1.74 (0.50)	1.70 (1.06)
HLSFA 3.0	18.3 (0.4)	8.9 (0.7)	1.63 (0.91)	1.36 (0.80)

The low strength of the LLSMK 3.0 sample is likely due to the higher water content used in the mixture leading to incomplete alkali-activation of the matrix supported by the leaching of free alkali in the form of efflorescence on the surfaces of the specimens after curing. LLSMK calcined samples exhibited extensive cracking after calcining and consequently, a strong decrease in compressive strength was measured (Fig. 22).

All FA based samples exhibited lower compressive strength than that of the MK based samples. However, LLSFA and HLSFA do not show evidence of cracking after calcining in the longitudinal or radial direction (Fig. 23 a, b).

In general, there was an increase in the compressive strengths after calcination in LLSFA samples in good agreement with the detected increased density (Tab. 5).

All LLSFA samples showed a compressive strength gain ranging from +86 % up to +188 %, the highest values being found for samples with higher Si/Al ratio.

Fig. 22: From the left: samples LLSMK 2.0, 2.5 and 3.0 after thermal treatment

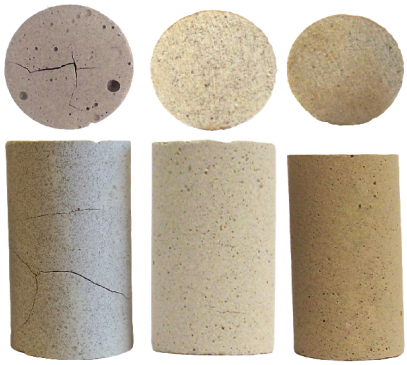

Fig. 23 a: From the left: samples LLSFA 2.0, 2.5 and 3.0 after thermal treatment

HLSFA samples exhibited an opposite trend, as they all experienced a sharp strength decrease, as well as considerable morphology changes and a slight density reduction after calcination. The different trend of compressive strength of calcined sample LLSFA and HLSFA can be ascribed to the unlike structure and nature of the crystalline phases formed during the thermal treatment.

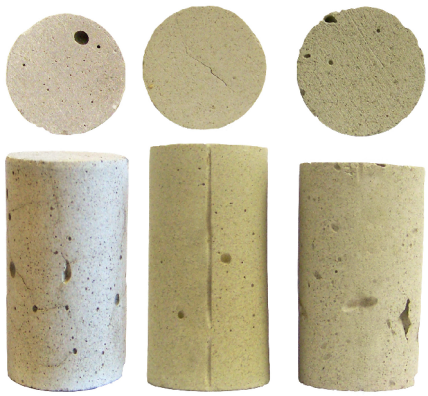

Fig. 23 b: From the left: samples HLSFA 2.0, 2.5 and 3.0 after thermal treatment

4.3.5 Microstructural properties after thermal exposure

Lower strength values recorded for calcined LLSMK samples might be related to changes in the microstructure occurred after heating. Crystallization of new phases, decomposition of calcium carbonate and changes in the pore structure are all factors that might have caused sample cracking and strength losses. Fig. 12 compares LLSMK 2.0 sample before and after calcination process. A compact microstructure is transformed into a porous microstructure where large pores, caused by gases released at high temperature, are evident in Fig. 12b, thus supporting the macroscopic cracks formation visible in Fig.10. Small pores of LLSMK might also have experienced high capillary strains during the dehydration process [76, 77], promoting their expansion (Fig. 24 a, b).

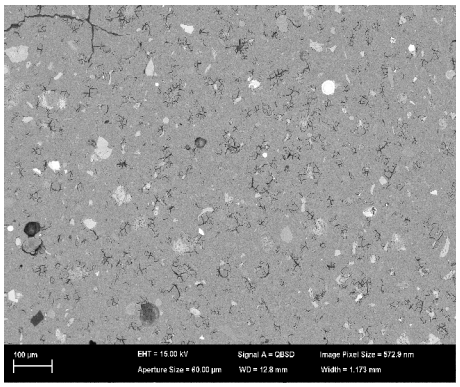

a

Fig. 24 a: Sample LLSMK 2.0 before thermal treatment (100X)

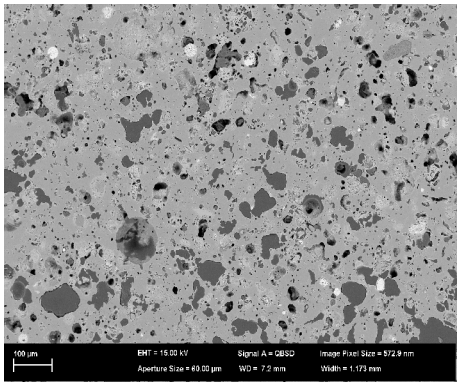

b

Fig. 24 b: Sample LLSMK 2.0 after thermal treatment (100X)

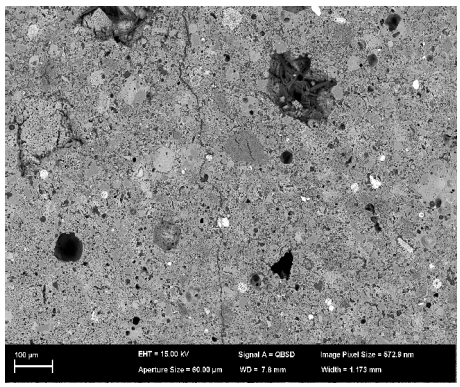

a

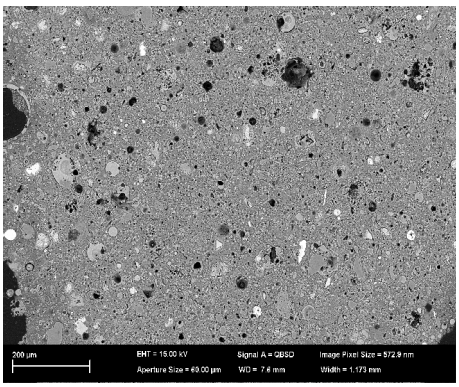

b

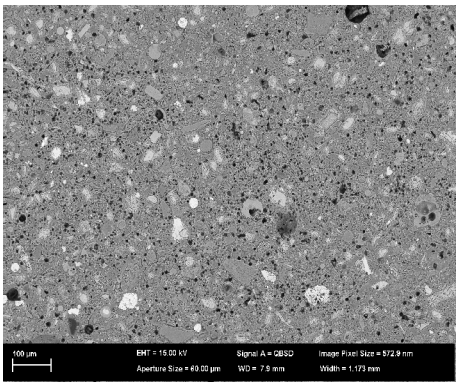

c

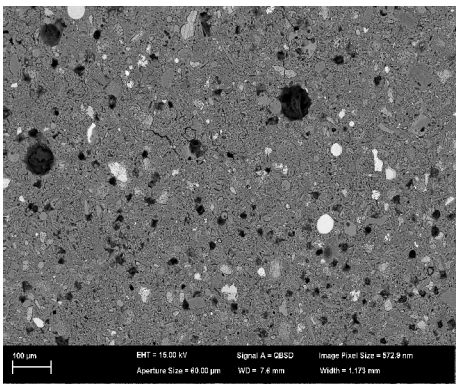

d

Fig. 25: SEM observation of LLSFA 2.0 (a, b) and, LLSFA 3.0 (c, d), 100 X. a, c = untreated; b, d = calcined

For FA based samples, microstructural changes after thermal treatment to 1000 °C is related to the LS content in the mixes (Fig. 25, 26). As general trend, calcining treatment increases sample porosity, however such increase is particularly evident for HLSFA (Fig. 26 b, d) compared to LLSFA (Fig. 25 b, d).

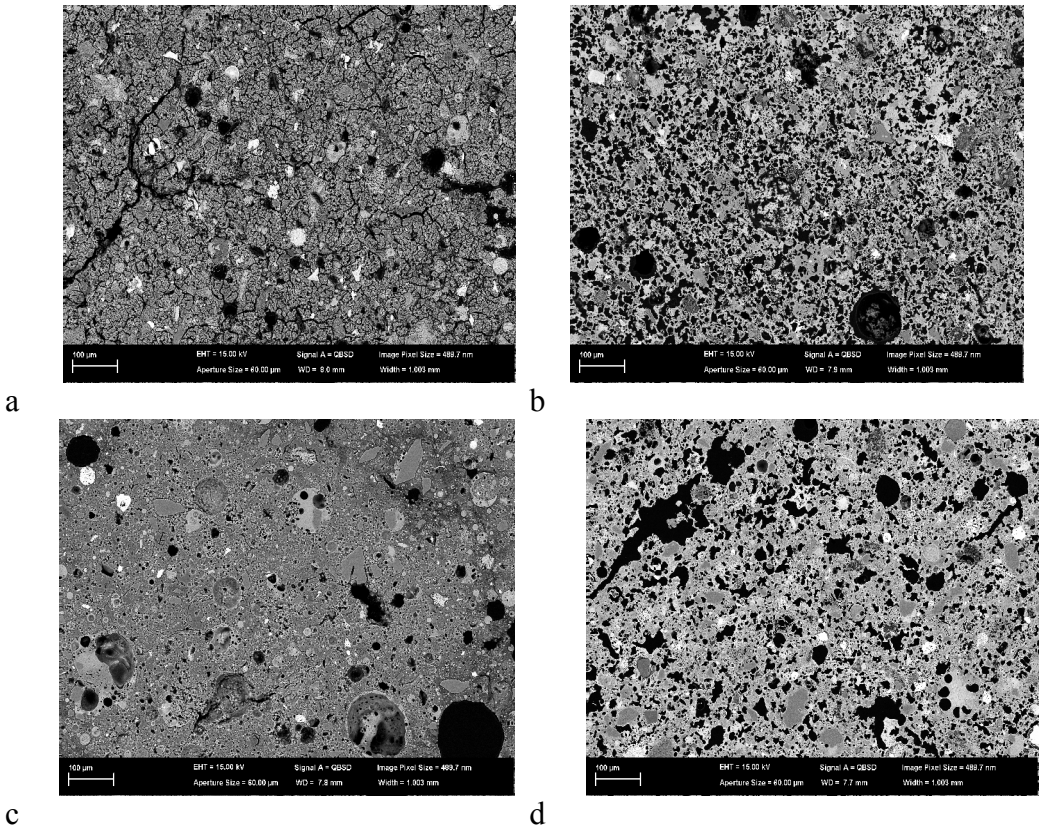

Fig. 26: SEM observation of HLSFA 2.0 (a, b) and, HLSFA 3.0 (c, d), 100 X.
a, c = untreated; b, d = calcined

Porosimetry analysis conducted on untreated and calcined LLSMK 2.0 samples (Fig.27) show a slight reduction in the total pore volume for thermal treated samples, suggesting that a sintering process might have occurred in the geopolymer gel. Densification of calcined LLSMK 2.0 is confirmed by an increased value of apparent density after heating (Tab. 12), as well as by a sharp shrinkage experienced by the samples during dilatometry tests, probably due to the dehydration of amorphous

calcium silicate phases and sintering of the gel. A fine and well reacted microstructure, with small and dispersed pores (Fig. 24, 27), is in facts believed to be more prone to condense and, thus, to show higher thermal shrinkage after heating.

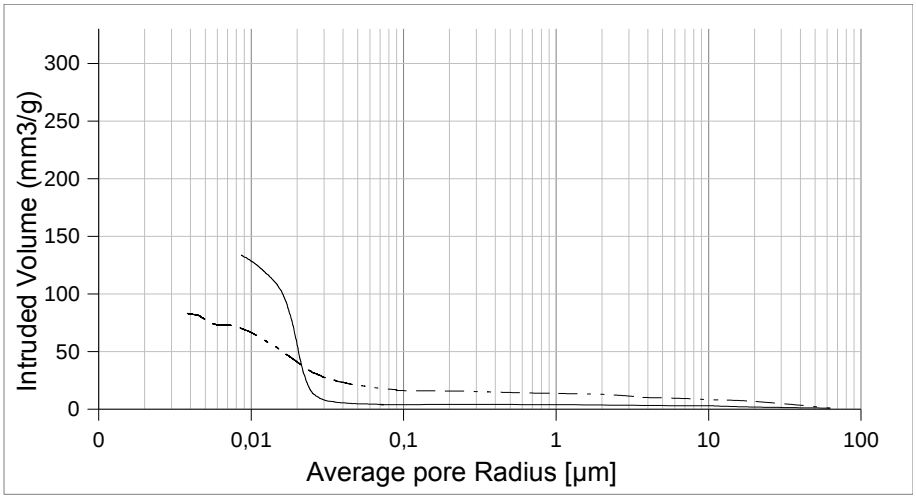

Fig. 27: Pore size distribution for untreated (black line) and calcined (dashed line) LLSMK 2.0

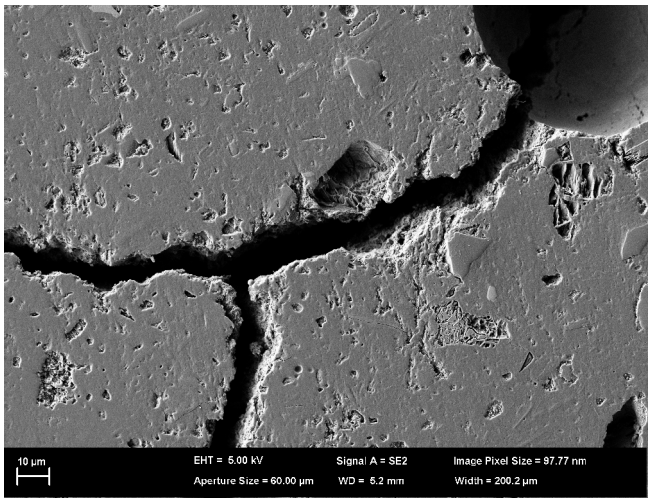

Fig. 28: SEM observation for sample LLSMK 2.0 after calcination, 500 X

Despite the reduction of total open porosity, a slight increase of macropores (> 0,05 μm) can be observed. However, the relatively small amount of these new-generated pore structures did not seem to have promoted the complete dissipation of gases produced upon heating, thus causing the samples to crack widely after calcination (Fig. 28). Smaller pores are in facts believed to suffer higher capillary strains: it is probable that the gel's pore structure was not able to cope with the tensile forces associated with high capillary strains during the dehydration process [76, 77] and it might have caused the samples to crack.

Pore size distribution for untreated and calcined LLSFA and HLSFA samples is reported below (Fig. 29-32). Contrarily to LLSMK mixtures, both LLSFA and HLSFA mixtures experienced an increase of the total open porosity after being calcined.

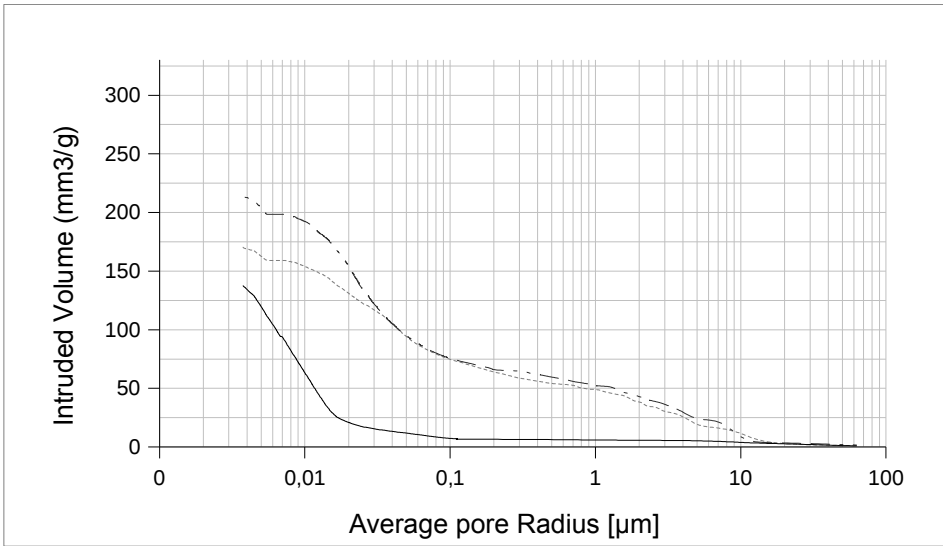

Fig. 29: Pore size distribution for untreated LLSFA 2.0 (black line), LLSFA 2.5 (black dashed line) and LLSFA 3.0 (gray dashed line)

As previously found for LLSMK samples, generally the thermal treatment does not only result in a change of the total intruded volume, but significantly affects also the pore size distribution, thus conditioning the mechanical performance after heating and the dimensional stability of the samples at high temperatures.

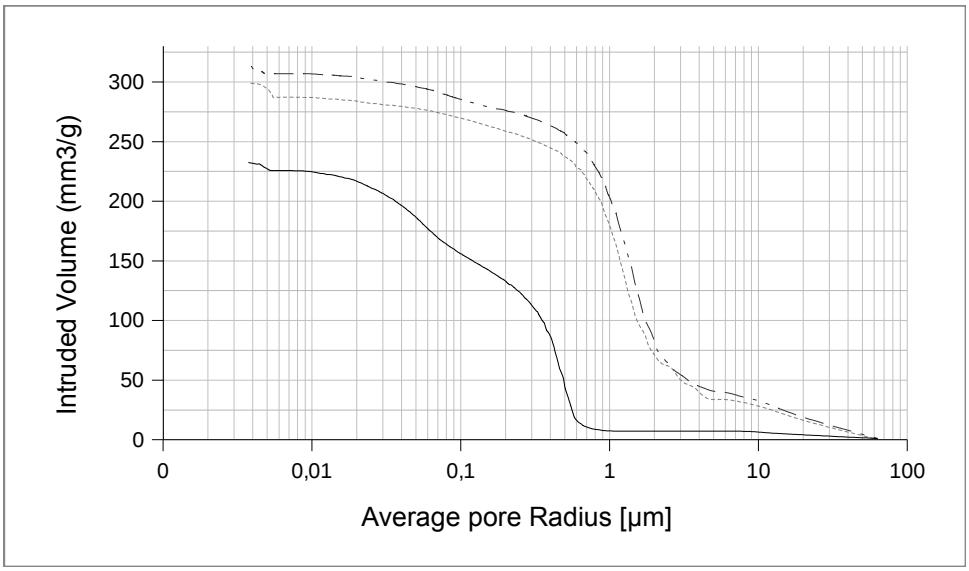

Fig. 30: Pore size distribution for treated LLSFA 2.0 (black line), LLSFA 2.5 (black dashed line) and LLSFA 3.0 (gray dashed line)

In facts, both fly-ash based mixtures could bear the final temperature of 1000°C without cracking as LLSMK did, thus suggesting that the pore network that evolves and generates during calcination can affect significantly the final physical and mechanical behaviour of the treated samples.

Compared to the other mixtures, LLSFA samples experienced slighter density changes after thermal treatment: the coalescence of micropore network and the simultaneous increase of macropores did not vary excessively the total amount of open porosity (Fig. 29-30). It is believed that a peculiar microstructure, defined by a

denser vitreous matrix together with a new generated pore structure, able to dissipate the gas produced from carbonate phases decomposition, can strongly enhance the mechanical performance of the samples after heating (Tab. 12).

HLSFA samples experienced considerable morphology changes and an apparent density reduction that might be related to a stronger increase in porosity, as found from the curves reported in Fig. 31-32, thus suggesting that the sintering process did not occur. As already mentioned, the higher amount of formed wollastonite and gehlenite is able to limit the paste's shrinkage and grant an enhanced dimensional stability (Fig. 17 c), even though it lowers the mechanical performance by opening the macropore network (Fig. 26 b, d).

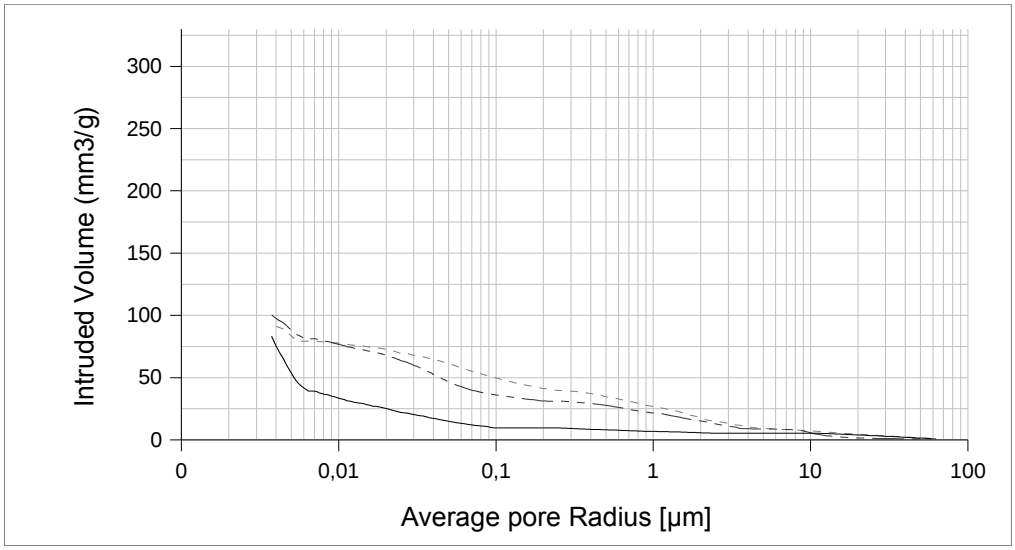

Fig. 31: Pore size distribution for untreated HLSFA 2.0 (black line), LLSFA 2.5 (black dashed line) and LLSFA 3.0 (gray dashed line)

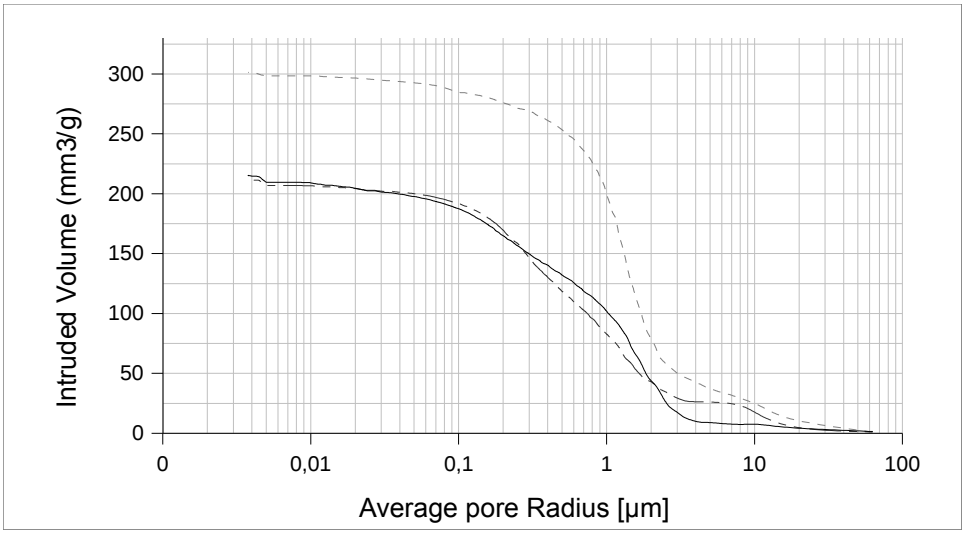

Fig. 32: Pore size distribution for treated HLSFA 2.0 (black line), LLSFA 2.5 (black dashed line) and LLSFA 3.0 (gray dashed line)

4.4 Corrosion resistance of alkali-activated steel reinforced mortars

4.4.1 Mechanical properties

Flexural (R_f) and compressive (R_c) strength of alkali-activated mortars has been obtained for all samples cured at ambient temperature (20± 2°C) in humid conditions (RH> 90%) for 7 days. Results are summarized in Table 13.

OPC mortars (M-CEMII-7) exhibited the highest values for both flexural and compressive strength, being 8.4 and 48.6 MPa, respectively. Alkali-activated mortars highlighted a different mechanical behaviour, depending on the specific LS amount used in the mix design: high-calcium based mortars (M-HLSFA 2.0-7) showed

reduced mechanical strength values, both for flexural and compressive strength, being respectively 6 and 2 times lower than normal OPC mortars.

Table 13: Mechanical properties of alkali-activated mortars

Samples	Curing time [days]	R_f [MPa]	R_c [MPa]
M-LLSFA2.0-7	7	4.3	38.6
M-HLSFA2.0-7	7	1.4	24.0
M-CEMII-7	7	8.4	48.6

Low-calcium based mortars (M-LLSFA 2.0-7) presented higher values of strength (4.3 and 38.6 MPa for R_f and R_c respectively), but still lower than cementitious mortars M-CEMII (Tab. 13).

4.4.2 Corrosion tests

As an accelerated corrosion test, IV technique has been performed on samples at different curing times (Tab. 14), by applying a determined potential difference to the steel bars. A measure of the actual speed of corrosion process has been given by plotting induced current intensity versus time: data for 7 and 21 or 28 days cured LS/FA-based mortar samples are reported in Fig. 35 and 36.

Generally, a first decreasing path can be observed for all samples, regardless the effective curing time, corresponding to the time needed from the steel bars to passivate. After the formation of the first corrosion film and, hence, after a relative

stability of the formed corrosion products, a sudden increase in current intensity values, indicative of the resumption of corrosion activity, can be noticed. This highlighted behaviour arises and develops differently for all samples and is strictly related to each sample's curing time [82]. Both 7 days cured M-LLSFA 2.0-7 (Fig. 33) and M-HLSFA 2.0-7 (Fig. 34) samples experienced a quick recovery of the corrosion activity, showing a remarkable instability even after the first 24 hours. The occurring current intensity increase is hence found to be closely related to the sample microstructure and, more specifically, is found to depend on the degree of geopolymerization of the mortar. A longer cured and, hence, a more homogeneous, and well reacted microstructure indeed results in an improved resistance to the occurrence of corrosion in the reinforcements. M-LLSFA 2.0-21 samples (Fig. 33), indeed, exhibited an increase of the current activity after the 5th day, while M-HLSFA-21 samples (Fig. 34), after showing a slight instability between 24 and 48 hours, registered an increase in current intensity after the 4th day. This confirms that corrosion occurrence is more easily promoted where the alkali-activation process and hydration reactions have not occurred completely.

OPC based mortars (Fig. 35) seem to be less influenced by specimens' curing time. M-CEMII-7 and M-CEMII-28 mortars, indeed, show a pretty similar behaviour, as evidences of corrosion occur around the 3rd day of test for 7 and 28 days cured mortars, remaining almost irrelevant the specific curing time. This confirms that alkali-activated LS/FA based materials, compared to traditional cementitious binders, can generate a less permeable microstructure in shorter times. With increasing curing time, they can in facts develop a more compact microstructure, thus showing an enhanced resistance to corrosion, even after 21 days of curing.

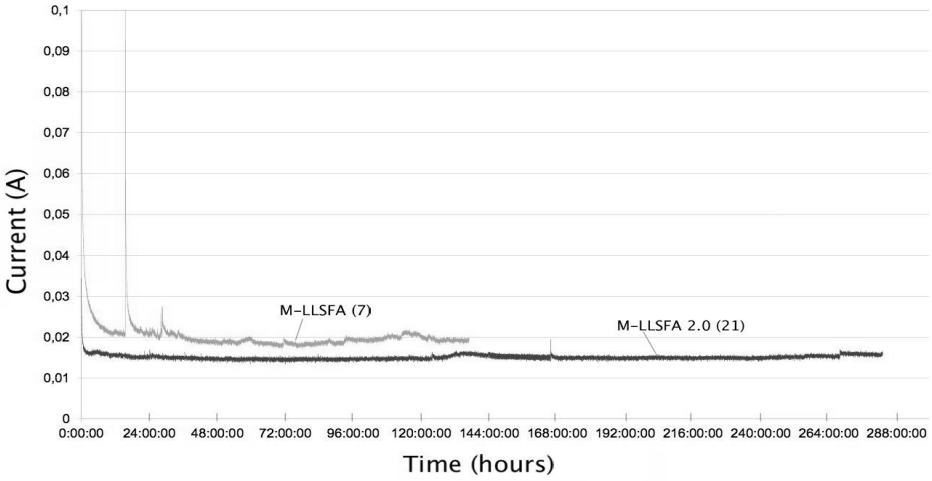

Fig. 33: Current-time plot at constant voltage of 5 V of reinforcing steel bar embedded in M-LLSFA 2.0 mortar samples at different curing time

As for alkali-activated mortars, significant differences can be evidenced in the corrosion resistance behaviour regarding different LS and FA amounts used in the mixtures. These differences appear more markedly for longer cured samples.

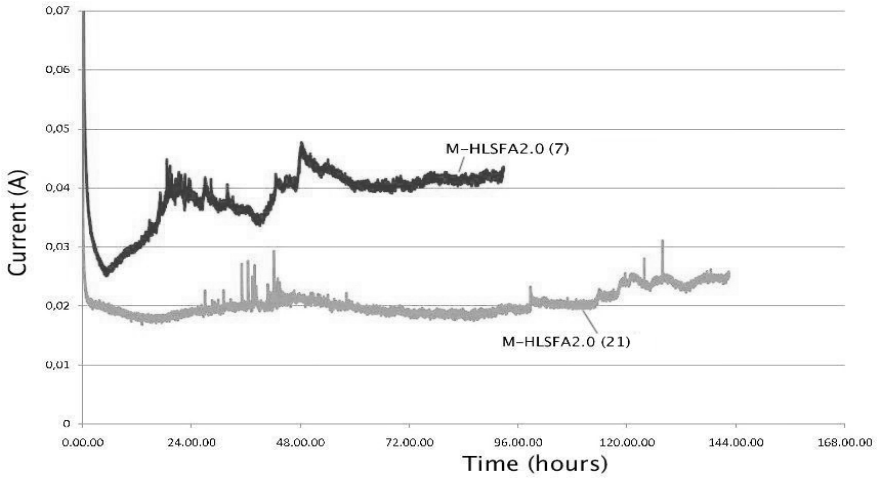

Fig. 34: Current-time plot at constant voltage of 5 V of reinforcing steel bar embedded in M-HLSFA2.0 mortar samples at different curing time

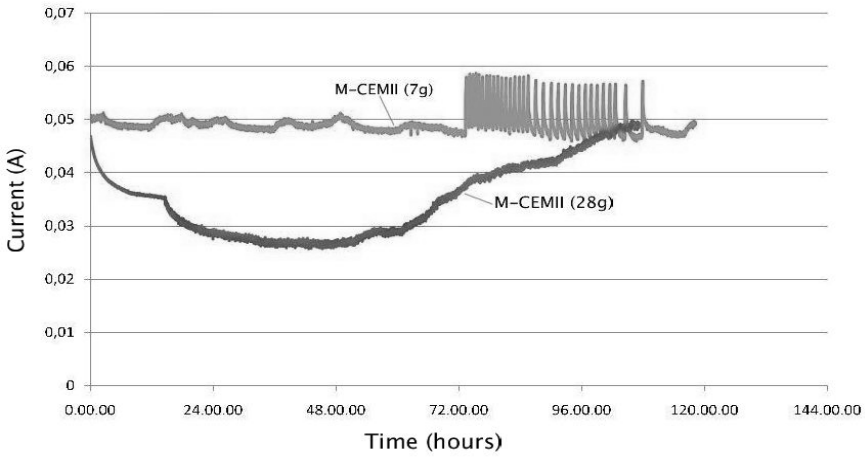

Fig. 35: Current-time plot at constant voltage of 5 V of reinforcing steel bar embedded in M-CEMII mortar samples at different curing time

An improvement in the onset time of corrosion can be evidenced for samples formulated with lower amounts of LS and, consequently, with lower contents of CaO in the starting materials (series M-LLSFA 2.0). These results thus suggest that FA, compared to LS, can contribute to a greater extent to obtain a more close-grained microstructure for longer curing times, thus substantially improving corrosion resistance and mortars durability.

The above commented data can be confirmed by analysing polarization resistance (R_p) data, recorded by LPR after IV test, that give information about the velocity of corrosion occurrence (Tab. 14).

R_p represents the ratio between the potential shift ΔE and the corresponding current change ΔI in an experimental polarization test within a few millivolts (± 25 mV) of the corrosion potential.

Table 14: Polarization resistance, chlorides for alkali-activated mortars

Samples	Curing time [days]	Rp (by LRP) [μA]
M-LLSFA 2.0 (7)	7	46.04
M-LLSFA 2.0 (21)	21	231.20
M-HLSFA 2.0 (7)	7	12.08
M-HLSFA 2.0 (21)	21	26.68
M-CEMII (7)	7	90.04
M-CEMII (28)	28	101.84

Polarization resistance is related to the steel corrosion current intensity by an inversely proportional relationship that means that the higher the Rp values, the slower the corrosion velocity for steel reinforced mortars samples.

OPC based mortars exhibit in facts Rp values of 90.0 and 101.8 μA for 7 and 28 days cured samples, highlighting a very similar corrosion speed rate. Among all 7 days cured samples, M-CEMII-7 showed the best behaviour, as Rp values for M-LLSFA 2.0-7 and M-HLSFA 2.0-7 were found to be significantly lower, suggesting that for short curing times OPC mortars can ensure a better corrosion protection to steel rebars. For longer cured samples, an increase in polarization resistance values was noticed for all specimens, in different extents regarding their specific formulation. Cementitious mortar samples (M-CEMII-28) exhibited just a 10% increase in Rp values compared to 7 days cured specimens, while high-calcium alkali-activated mortar samples (M-HLSFA 2.0-21), despite they exhibited a 55% increment in Rp values, showed a final value of 26.7 μA, still lower than that found for cementitious mortar samples. Low-calcium alkali-activated mortar samples (M-LLSFA 2.0-21) greately increased their polarization resistance values with increasing specimens

curing time from 7 to 21 days: an 80% increment for R_p values was registered for 21 days cured samples compared to 7 cured ones, thus confirming that a significant drop in corrosion rate has occurred, leading to a much better corrosion resistance of steel reinforcement than that promoted by OPC and high-calcium alkali-activated mortar samples.

4.4.3 Microstructural characterization

Pore size distributions have been determined for cementitious and alkali-activated mortar samples after IV and LPR tests. Results are reported in fig. 36 and 37; cumulative pore volume and average pore radius values for all investigated samples are summarized in Table 15.

All samples from M-CEMII, M-LLSFA 2.0 and M-HLSFA 2.0 series show an evident reduction in cumulative pore volume with increasing specimens curing time, and they all exhibit pore size distributions that become smaller moving from 7 days to 21 or 28 days cured samples. This reduction becomes more evident for M-LLSFA 2.0 and M-HLSFA 2.0 samples, where the cumulative pore volume undergoes a decrease of 30 and 36% respectively with passing from 7 days to 21 days cured samples, while M-CEMII samples experienced only a 14% reduction.

Despite M-CEMII showed the lowest value for shortly-cured specimens, it is worth to note that for longer curing times low-calcium alkali-activated mortars (M-LLSFA 2.0-21) come to have a lower value of cumulative pore volume, confirming how much importance does curing time have for these kind of mortars in generating a less porous microstructure.

Table 15: Polarization resistance for cementitious and alkali-activated mortars after IV and LPR test

Samples	Cumulative pore volume [mm^3/g]	Mean pore radius [µm]	Cl^- [%]	PH at 24.2±0.2°C
M-LLSFA 2.0 (7)	74.15	2.332	0.25	8.8
M-LLSFA 2.0 (21)	51.28	0.122	0.23	10.8
M-HLSFA 2.0 (7)	154.74	8.180	0.52	9.4
M-HLSFA 2.0 (21)	97.57	3.121	0.54	8.6
M-CEMII (7)	64.89	0.038	0.54	7.0
M-CEMII (28)	55.96	0.032	0.50	8.0

For alkali-activated mortars (M-LLSFA 2.0 and M-HLSFA 2.0 series), a sharp reduction in the mean pore radius was also noticed with increasing specimens' curing time. M-CEMII samples, instead, maintained almost the same value of mean pore size, being however considerably lower than for alkali-activated mortars.

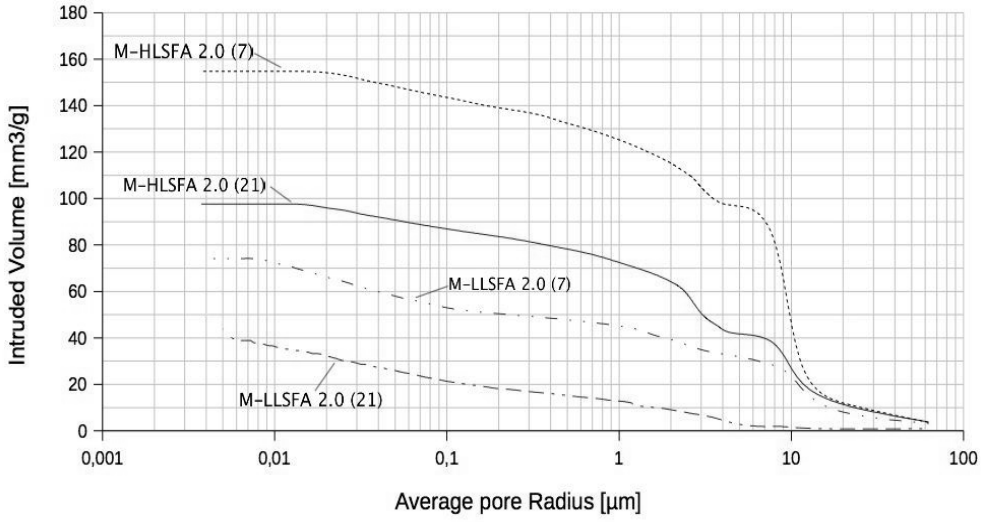

Fig. 36: Pore size distribution for 7 and 21 days cured M-LLSFA 2.0 and M-HLSFA 2.0 mortar samples after IV test

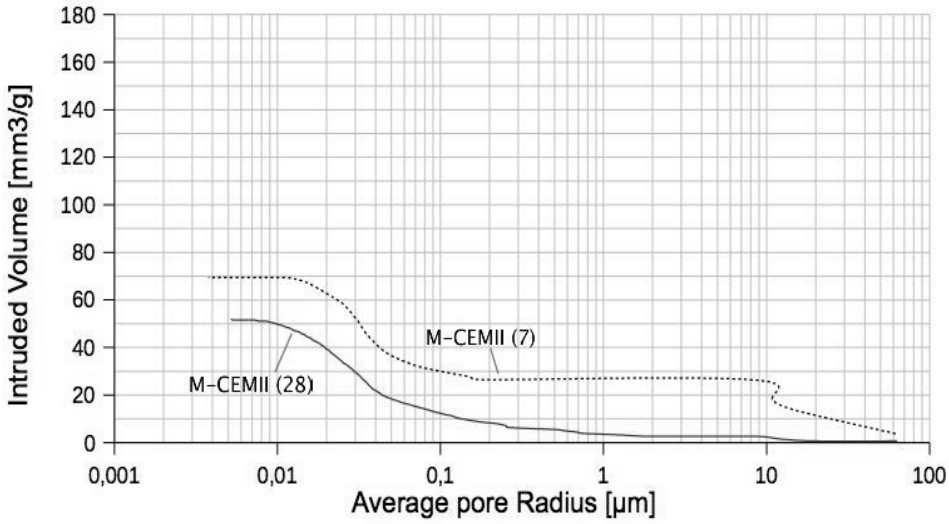

Fig. 37: Pore size distribution for 7 and 28 days cured M-CEMII mortar samples after IV test

The mean pore radius is defined as the pore radius at which 50% of the pore volume is intruded in the pore size range considered, and pretty much corresponds to the critical pore radius, the latter being the smallest pore size diameter of the subset of the largest pores which creates a connected path through the sample. As such, the critical pore radius plays an important role in defining the specimen's behaviour towards transportation and diffusion of soluble salts, and values of mean pore radius can hence give a direct indication about these compounds diffusion process through the mortars. Therefore, corrosion behaviour of rebars is strictly related to the content of Cl^- ions (coming from the NaCl solution in which specimens are dipped) that can penetrate into the mortar by diffusion process, which is in turn proportionally related to the mean pore radius.

Chloride content and pH values, determined after LPR test for all specimens, are summarized in Table 15.

a

a

c

Fig. 38: Corrosion evidences (top and lateral surfaces) on M-LLSFA 2.0-7 (a), M-HLSFA 2.0-7 (b), M-CEMII-7 (c)

For all investigated samples pH values lies in the range of 7.0–10.8. Lower values are associated to higher corrosion risk: the lower the pH, the lower the threshold limit for de-passivation of rebars by chloride attacks [83]. Ferrous and ferric oxides are not protective anymore at pH levels less than approximately 11.5 [84]: the relatively high value of pH and a low chlorides concentration found in M-LLSFA 2.0-21 sample highlighted that this specimen had the best corrosion resistance above all other investigated samples. Chlorides content was found ranging from 0.23% (M-LLSFA 2.0-21 to 0.54% (M-HLSFA 2.0-21 and M-CEMII-7) over the total binder content. Cementitious and high-calcium alkali-activated mortars exhibited quite similar contents, stated around 0.52% (±0.02), regardless the curing time of the specimens.

Chlorides concentration for low-calcium alkali-activated mortars (M-LLSFA 2.0 series) were found to be significantly lower than for other samples, being 0.25 and 0.23% for 7 and 21 days cured samples respectively. A superior chloride permeation resistance exhibited by alkali-activated mortars compared to OPC based ones can be pointed out, likely to be due to a lower chloride diffusion coefficient for the former [85].

A qualitative analysis on mortar specimens after IV and LPR test can be done to assess evidences of corrosion: the way in which it occurs, by generating brown stains and rusty deposits on side surface area and/or on top surface and longitudinal cracks along the side area can give information about ions migrations and diffusion process through the mortars. Corrosion evidences on M-HLSFA 2.0 and M-CEMII samples generally appeared on lateral surfaces of the specimens, causing the samples to crack along their side (Fig. 38 b, c and 39 b, c).

a

b

c

Fig. 39: Corrosion evidences (top and lateral surfaces) on M-LLSFA 2.0-21 (a), M-HLSFA 2.0-21 (b), M-CEMII-21 (c)

Wide brown stains and rust deposits can be observed on all samples' surfaces, more remarkably for 7 days cured samples, M-HLSFA 2.0-7 and M-CEMII-7. Contrarily, for both 7 and 21 days low-calcium mortar samples (M-LLSFA 2.0 series) corrosion signs appeared firstly on top surface, and only M-LLSFA 2.0-7 exhibited a slightly marked longitudinal crack (Fig. 38 a and 39 a).

These findings are consistent with previously commented data, suggesting that low-calcium alkali-activated mortars are more prone to form a less permeable microstructure than other investigated mortars, and that permeability to chlorides by ionic diffusion significantly decreases with increasing curing time. Corrosion evidences on the top surface area are likely to be associated with the development of a differential aeration cell occurring on the rebar due to some crevices between bar and mortar and only in negligible extent to ions migration from the solution to the mortar, as found for high-calcium M-HLSFA 2.0 and M-CEMII formulations.

5 Conclusions

This research demonstrated that the use of traditional and innovative sustainable binders in several building engineering application fields is possible. Substitution of traditional OPC binders with green alternative materials can indeed result in many different advantages in terms of a reduced environmental impact and carbon footprint, as well as higher performances and improved structural behaviour. Indeed, compared to commonly used cementitious binders, sustainable ones, such as lime or alkali-activated materials, highlighted a better compatibility with most of the architectural substrate materials and evidenced higher durability properties in most of the critical operating conditions they are used in. In details, the following considerations can be deduced.

Results obtained from the utilization of natural lime-based matrices for structural rehabilitation permit to assess the effective efficiency of the newly developed reinforcing method. The designed system, based on a non-invasive binding technology, indeed resulted in a more suitable, high performing, easy applicable and hazard-free repair material. The investigated lime-based matrix added with a specific water-dispersible polymer can in facts properly impregnate and cover the reinforcing

fiber fabrics and grant an adequate mechanical interlock with the substrate's superficial roughness, thus performing an efficient strengthening effect. Experimental results have shown that this lime-based binding matrix can be successfully used as a valid alternative for any other cement-based matrix compound. Samples strengthened with this innovative system, indeed, exhibited a similar behaviour to those reinforced with the traditional cement-based system in terms of load bearing increase capacity, adherence properties and ductility. Besides that, the developed system can ensure a better compatibility with most of the substrate materials that characterize the historical and ancient buildings, avoiding the use of any compound, such as cementitious binders, that could generate serious damages to the original material. Any mismatch between chemical, physical and mechanical properties between the substrate and the reinforcing elements might indeed generate undesirable effects, thus leading to an inefficient or even self-defeating intervention.

- Low-impact alkali-activated materials can be used as innovative matrices to cast high toughness inorganic composites for structural applications and repair interventions. Fiber-reinforced composite materials based on a ladle slag/metakaolin geopolymer matrix have been successfully designed. All the selected fibers (carbon, E-glass, PVC and PVA) were found to have good adhesion properties, being able to control micro-cracks propagation and creating a favourable bridging effect within the matrix. A better behaviour of carbon and polymer fibers has been generally observed in enhancing the material's toughness and ductility upon failure compared to glass ones. Moreover, it has been found that a fraction equal to 1% wt. of reinforcing fibers embedded in the alkali-activated matrix is able to determine a flexural strength increment ranging from 30% up to 70%, depending on the fiber type, compared to

the plain unreinforced material. Alkali activated matrices added with PVC and carbon fibers exhibited the best energy absorption capacity: for these types of fibers the post-crack behaviour is significantly improved, resulting in an enhanced ductility of the material after reaching the first crack load.

- New sustainable and high performance binders for high temperature applications can be obtained from alkali-activation of only industrial wastes and by-products materials, such as ladle slag and fly ash. While fly ash contribute to enhance the material's properties at high temperatures, by promoting a densification and sintering process that helps to improve dimensional stability and compressive strength after heating, CaO-rich ladle slag can promote the formation of ambient-curing alkali activated materials, thus representing an outstanding advantage for building industry applications. However, free CaO content in raw materials significantly influences the reaction products of the pastes, thus affecting markedly the geopolymers physical, mechanical and microstructural properties at ambient and high temperature: the total amount of calcium oxide in the mix formulation should hence be taken into account before formulating a specific mix design, depending on the parameters and properties that it should comply with.

In details, it has been demonstrated that ladle slag can be considered an interesting alternative source of raw material for alkali-activation process and the investigated mix designs highlighted a better processability of ladle slag with fly ash compared to metakaolin. Calcium content plays an important role when thermal exposure is carried out. Calcined samples based on ladle slag and fly ash promoted the formation of new crystalline phases, which differ as function of calcium amount. The more calcium is present in the mix, the more gehlenite is formed, a substantially thermally

stable mineral compound. Samples based on ladle slag and fly ash exhibited a higher dimensional stability than those based on metakaolin. Indeed, as calcium amount increases, thermal shrinkage is hindered by the newly formed crystalline phase, but a decrease in compressive strength has been ascertained. The joint activation of ladle slag and fly ash generates a solid system that is based on the interaction of two different type of waste thus promoting the development of sustainable binder and representing an outstanding advantage for building industry applications.

- Waste materials as ladle slag and fly ash were demonstrated particularly suitable to be used as novel binding materials to formulate construction and repair mortars via alkali-activation. Both low-calcium and high-calcium mix designs obtained from ladle slag and fly ash blends were found to be completely compatible with embedded rebars and showed good adhesion properties to steel reinforcements. Low-calcium formulations also exhibited promising results in terms of mechanical properties, returning compressive and flexural strength values only slightly lower than those of OPC based mortars.

More markedly than for OPC mortars, specimens' curing time for geopolymer mortars was found to play a significant role in determining the material's microstructure, thus necessarily affecting its durability properties and its behaviour toward soluble salts penetration. All investigated samples showed indeed a remarkable reduction in cumulative pore volume with increasing curing time from 7 to 21 or 28 days. Geopolymer mortar formulations were finally demonstrated to have good corrosion resistance and durability properties: especially for longer cured samples, alkali-activated mortars exhibited a preferable behaviour in protecting the rebars against corrosion occurrence compared to traditional OPC mortars. Ladle slag

and fly ash based mortars indeed were able to generate a less porous microstructure in shorter times, granting a lower chlorides permeability through the material, thus enhancing steel reinforcements corrosion resistance. The higher pH values and lower chlorides concentrations detected on tested low-calcium alkali-activated mortar samples highlighted a better behaviour for these formulations, referring to high-calcium and cementitious ones. Therefore, these findings lead to consider fly ash, and secondly ladle slag, particularly apt to yield a less permeable and a more close-grained material, thus confirming that a more sustainable and performing material can be obtained by alkali-activation of alumino-silicate wastes and by-products.

6 References

[1] G. Marazzi, Impatto dell'Emissions Trading sull'industria italiana del cemento, Proceedings of Milan Climate Change Conference, AITEC, Milano, 29-30 Novembre (2004)

[2] N. Müller, E. Bollin, J.Harnisch, A blueprint for a climate friendly cement industry, WWF International report, in The Poznan Climate Change Conference, 1-12 December (2008) Poznan, Poland

[3] AA.VV., CO_2 and Energy Accounting and Reporting Standard for the Cement Industry, Protocol from WBCSD-Cement Sustainability Initiative (CSI), May (2011)

[4] P. Duxon, J. Provis, Low CO_2 concrete: are we making any progress?, BEDP Environment Design Guide, Paper PRO24. Australian Institute of Architects, Melbourne, Australia (2009)

[5] A. Rattazzi, C. Polidoro, La calce nel sistema LEED. Un materiale antico con un futuro 'verde' e 'sostenibile', Forum Italiano Calce News, Aprile (2010) 1-8

[6] L. Zongjin, D. Zhu, Z. Yunsheng, Development of sustainable cementitious

materials, Proceedings from International Workshop on Sustainable Development and Concrete Technology, Beijing, China, May 20–21 (2004) 55-76

[7] J. Davidovits, Geopolymers: man-made rock geosynthesis and the resulting development of very early high strength cement, Journal Mater Ed 16 (1994) 91- 139

[8] V.D. Glukhovsky, G.S. Rostovskaya, G.V. Rumyna, High Strength Slag- Alkaline Cements, Proceedings of he 7th International Congress on the Chemistry of Cement, Paris, 3 (1980) 164-168

[9] V. Medri, Geopolimeri: “Ceramiche” per uno sviluppo sostenibile, L’Industria dei Laterizi 115 (2009) 48-53

[10] P. Duxson, A. Fernandez-Jimenez, J.L. Provis, G.C. Lukey, A. Palomo, J.S.J. van Deventer, Geopolymer technology: the current state of the art, Adv Geop Sci Tech 42 (2007) 2917-2933

[11] J. Davidovits, 30 Years of Successes and Failures in Geopolymer Applications. Market Trends and Potential Breakthroughs, Geopolymer 2002 Conference, October 28-29 (2002) Melbourne, Australia, 1-16

[12] P. Duxson, G.C. Lukey, J.S.J. Van De Venter, S.W. Mallicot, W.M. Kriven, Microstructural characterisation of metakaolin-based geopolymers, Ceram Trans 165 (2005) 71-85

[13] A.V. Kirschner, H. Harmuth, Investigation of geopolymer binders with respect to their application for building materials, Ceram Silikaty 48 (2004) 117-120

[14] C.K. Yip, J. Provis, G.C. Lukey, J.S.J. Van Deventer, Carbonate mineral addition

to metakaolin-based geopolymer,. Cement Concrete Comp 30 (2008) 979-985

[15] P. Duxson, J. L. Provis, Designing Precursors for Geopolymer Cements, Journal of American Ceramic Society, 91 (2008) 3864-3869

[16] W.D.A. Rickard, A. Van Riessen, P. Walls, Thermal Character of Alkali-activated materials Synthesized from Class F Fly Ash Containing High Concentrations of Iron and a-Quartz, Int. J. Appl Ceram Technol 7 (2010) 81-88

[17] K. Dombrowski, A. Buchwald, M. Weil, The influence of calcium content on the structure and thermal performance of fly ash based geopolymers, J Mater Sci 42 (2007) 3033-3043

[18] M. Guerrieri, J.G. Sanjayan, Behaviour of combined fly ash/slag-based geopolymers when exposed to high temperatures, Fire Mater 34 (2010) 163-175

[19] L. Zuda, P. Rovnanik, P. Bayer, R. Černý, Thermal properties of alkali-activated slag subject to high temperatures, J Build Phys 30 (2007) 337-350

[20] A. Buchwald, H. Hilbig, Ch. Kaps, Alkali-activated metakaolin-slag blends—performance and structure in dependence of their composition, J Mater Sci 9 (2007) 3024-3032

[21] M. Weil, K. Dombrowski, A. Buchwald, Ecological and economic analyses of geopolymer concrete mixes for external structural elements, ZKG International 64 (2011) 76-87

[22] B. C. McLellan, R. P. Williams, J. Lay, A. van Riessen, G. D. Corder, Costs and carbon emissions for geopolymer pastes in comparison to ordinary Portland cement,

Journal of Cleaner Production 19 (2011) 1080-1090

[23] A. Kalagri, A. Miltiadou-Fezans, E. Vintzileou, Design and evaluation of hydraulic lime groutsfor the strengthening of stone masonry historic structures, Materials and Structures 43 (2010) 1135-1146

[24] J. Lanas, J.L. Pérez Bernal, M.A. Bello, J.I. Alvarez Galindo, Mechanical properties of natural hydraulic lime-based mortars, Cement and Concrete Research 34 (2004) 2191-2201

[25] S. Pavìa, R. Hanley, Flexural bond strength of natural hydraulic lime mortar and clay brick, Materials and Structures 43 (2010) 913-922

[26] T. Hanzlicek, M. Steinerova, P. Straka, I. Perna, P. Siegl, T. Svarcova, Reinforcement of the terracotta sculpture by geopolymer composite, Materials and Design 30 (2009) 3229-3234

[27] B. Fabbri, S. Gualtieri, Impiego di materiali geopolimerici come adesivivi nella conservazione di manufatti in pietra naturale o artificiale, Atti del IV Convegno "Monitoraggio e Conservazione preventiva dei Beni Culturali", 27-29 Maggio (2010) 15-22

[28] S. Rescic, P. Plescia, P. Cossari, E. Tempesta, D. Capitani, N. Proietti, F. Fratini, A.M. Mecchi, Mechano-chemical activation: an ecological safety process in the production of materials to stone conservation, Procedia Engineering 21 (2011) 1061-1071

[29] C. Leonelli, M. Romagnoli, Geopolimeri Polimeri Inorganici Chimicamente Attivati, Lulu ed., (2011) pp. 287

[30] J.W. Giancaspro, C.G. Papakonstantinou, P.N. Balaguru, Flexural Response of Inorganic Hybrid Composites With E-Glass and Carbon Fibers, Journal of Engineering Materials and Technology 132 (2010) 51-58

[31] R. E. Lyon, P. N. Balaguru, A. Foden, U. Sorathia, J. Davidovits, M. Davidovics, Fire-resistant Aluminosilicate Composites, Fire and Materials, 21 (1997) 67-73

[32] H. Peigang, J. Dechang, L. Tiesong, W. Meirong, Z. Yu, Effects of high-temperature heat treatment on the mechanical properties of unidirectional carbon fiber reinforced geopolymer composites, Ceramics International 36 (2010) 1447-1453

[33] S.L. Yong, D.W. Feng, G.C. Lukey, J.S.J. van Deventer, Chemical characterization of the steel–geopolymeric gel interface, Colloids and Surfaces A: Physicochem. Eng. Aspects, 302 (2007) 411-423

[34] J.M. Miranda, A. Fernández-Jiménez, J.A. Gonzalez, A. Palomo, Corrosion resistance in activated fly ash mortars, Cement and Concrete Research 35 (2005) 1210-1217

[35] Sofi, M., van Deventer, J. S. J., Mendis, P. A. and Lukey, G. C., Bond performance of Reinforcing Bars in Inorganic Polymer Concrete (IPC), Journal of Materials Science 42(2007) 3107-3116

[36] Sarker, P. K., Grigg, A. and Chang, E.H., Bond Strength of Geopolymer Concrete with Reinforcing Steel, Proceedings of Recent Development in Structural Engineering, Mechanics and Computation, Ed. Zingoni (2007) 1315-1320

[37] G. Manfredi, L. Ascione, Innovative materials for the vulnerability mitigation of existing structures, in ReLuis-DPC Project Final Report, Napoli (2009) 1-53

[38] B. Täljsten, The importance of bonding-a historic overview and future possibilities, Advances in Structural Engineering 9 (2006) 721-735

[39] C. Pellegrino, F. Da Porto, C. Modena, Rehabilitation of reinforced concrete axially loaded elements with polymer-modified cementitious mortar, Construction and Building Materials 23 (2009) 3129-3137

[40] M. A. Aiello, S. M. Sciolti, Bond analysis of masonry structures strengthened with CFRP sheets, Construction and Building Materials 20 (2006) 90-100

[41] T.C. Triantafillou, C.G. Papanicolaou, Textile Reinforced Mortars (TRM) versus Fiber Reinforced Polymers (FRP) for Concrete Confinement, in Proceedings of 7th International Symposium on Fiber-Reinforced (FRP) Polymer Reinforcement for Concrete Structures, C. K. Shield, J. P. Busel, S. L. Walkup and D. D. Gremel, Editors, ACI Special Publication, MI, USA (2005) 99-118

[42] H. Toutanji, Y. Deng, Comparison between organic and inorganic matrices for RC beams strengthened with carbon fiber sheets, Journal of Composites for Construction 11 (2007) 507-513

[43] S. Kurtz, P. Balaguru, Comparison of inorganic and organic matrices for strengthening of RC beams with carbon sheets, Journal of Structural Engineering 127 (2001) 35-42

[44] S. Xu, M. Krüger, H. W. Reinhardt, J. Ozbolt, Bond characteristics of carbon,

alkali resistant glass, and aramid textiles in mortar, Journal of Materials in Civil Engineering 16 (2004) 356-364

[45] O. Weichold, M. Möller, A cement-in-poly(vinyl alcohol) dispersion for improved fiber-matrix adhesion in continuous glass-fiber reinforced concrete, Advanced Engineering Materials 9 (2007) 712-715

[46] U. Dilthey, M. Möller, O. Weichold, Application of polymer in textile reinforced concrete - from the interface to construction elements, in Proceedings of 1st International Conference on Textile Reinforced Concrete - ICTRC, Aachen (2006) 1-11

[47] J.W. Giancaspro, C.G. Papakonstantinou, P.N. Balaguru, Mechanical behavior of fire-resistant biocomposite, Composites Part B: Engineering 40 (2009) 206-211

[48] F. De Caso y Basalo, F. Matta, A. Nanni, Fiber reinforced cementitious matrix composites for infrastructure rehabilitation, in Composites & Polycon 2009 Proceedings - American Composites Manufacturers Association - ACMA (2009) 1-12

[49] B. Täljsten, T. Blanksvärd, Mineral-based bonding of carbon FRP to strengthen concrete structures, Journal of Composites for Construction 11 (2007) 120-128

[50] H. Toutanji, L. Zhao, Y. Zhang, Flexural behavior of reinforced concrete beams externally strengthened with CFRP sheets bonded with an inorganic matrix, Engineering Structures 28 (2006) 557-566

[51] J. Hammell, P. Balaguru, R. Lyon, Influence of reinforcement types on the flexural properties of geopolymer composites, In Materials and process affordability

- Keys to the future; Proc. 43rd International SAMPE Symposium, May 31st – June 4th, Anaheim, CA (1998) 1600-1608

[52] Q. Zhao, B. Nair, T. Rahimian, P. Balaguru, Novel geopolymer based composites with enhanced ductility, Journal of Materials Science 42 (2007) 3131-3137

[53] F.J. Silva, C. Thaumaturgo, Fibre reinforcement and fracture response in geopolymeric mortars, Fatigue & Fracture of Engineering Materials & Structures 26 (2006) 167-172

[54] D.P. Dias, C. Thaumaturgo, Fracture toughness of geopolymeric concretes reinforced with basalt fibers, Cement and Concrete Composites 27 (2005) 49-54.

[55] H. Toutanji, B. Xu, J. Gilbert, T. Lavin, Properties of poly(vinyl alcohol) fiber reinforced high-performance organic aggregate cementitious material: Converting brittle to plastic, Construction and Building Materials 24 (2010) 1-10

[56] W. Li, J. Xu, Mechanical properties of basalt fiber reinforced geopolymeric concrete under impact loading, Materials Science and Engineering 505 (2009) 178-186

[57] T. Lin, D. Jia, P. He, M. Wang, In situ crack growth observation and fracture behaviour of short carbon fiber reinforced geopolymer matrix composites, Materials Science and Engineering A 527 (2010) 2404–2407

[58] Z. Zhang, X. Yao, H. Zhu, S. Hua, Y. Chen, Preparation and mechanical properties of polypropylene fiber reinforced calcined kaolin-fly ash based geopolymer, Journal of Central South University of Technology 16 (2009) 49- 52

[59] Z. Yunsheng, S. Wei, L. Zongjin, Z. Xiangming, C. Chungkong, Impact properties of geopolymer based extrudates incorporated with fly ash and PVA short fibers, Construction and Building Materials 22 (2008) 370-383

[60] B.I.G. Barr, K. Liu, R.C. Dowers, A toughness index to measure the energy absorption of fibre reinforced concrete, International Journal of Cement Composites and Lightweight Concrete 4 (1982) 221-227

[61] A. Buchwald, M. Shulz, Alkali-activated binders by use of industrial by-products, Cement Concrete Res 35 (2005) 968–973

[62] C.K. Yip, G.C. Lukey, J.L. Provis, J.S.J. Van Deventer, Effect of calcium silicate sources on geopolymerization, Cement Concrete Res 38 (2008) 554-564

[63] W.D.A. Rickard, R.P. Williams, J. Temuujin;, A. Van Riessen, Assessing the suitability of three Australian fly ashes as an aluminosilicate source for geopolymers in high temperature applications, Mater Sci Eng A-Struct 528 (2011) 3390-3397

[64] P. Duxson, S.W. Mallicoat, G.C. Lukey, W.M. Kriven, J.S.J. Van Deventer, J.S.J. The effect of alkali and Si/Al ratio on the development of mechanical properties of metakaolin-based geopolymers, Colloid Surface A: Physicochem. Eng. Aspects 292 (2007) 8-20

[65] M.C. Bignozzi, L. Barbieri, I. Lancellotti, New Geopolymers based on Electric Arc Furnace Slag, Advances in Science and Technology 69 (2010) 117-122

[66] S. Kourounis, S. Tsivilis, P.E. Tsakiridis, G.D. Papadimitriou, Z. Tsibouki, Properties and hydration of blended cements with steelmaking slag, Cement

Concrete Res 37 (2007) 815-822

[67] S. Caijun, Characteristics and cementitious properties of ladle slag fines from steel production, Cement Concrete Res. 32 (2002) 459-462

[68] J. Temuujin, A.Van Riessen, R.P. Williams, Influence of calcium compounds on the mechanical properties of fly ash geopolymer pastes, J Hazard Mater 167 (2009) 82-88

[69] F. Winnefeld, A. Leeman, M. Lucuk, P. Svoboda, M. Neuroth, Assessment of phase formation in alkali activated low and high calcium fly ashes in building materials, Constr Build Mater 24 (2010) 1086-1093

[70] C.K. Yip, J.S.J. Van Deventer, Microanalysis of calcium silicate hydrate gel formed within a geopolymeric binder. J Mater Sci 38 (2003) 3851-3860

[71] J. Tailby, K.J.D. MacKenzie, Structure and mechanical properties of aluminosilicate geopolymer composites with Portland cement and its constituent minerals, Cement Concrete Res 40 (2010) 787-794

[72] C.K. Yip, G.C. Lukey, J.S.J. Van Deventer, The coexistence of geopolymeric gel and calcium silicate hydrate at the early stage of alkaline activation, Cement Concrete Res 35 (2005) 1688-1697

[73] M. Guerrieri, J.G. Sanjayan, F. Collins, Residual strength properties of sodium silicate alkali activated slag paste exposed to elevated temperatures, Mater Struct 43 (2010) 765-773

[74] A. Mendes, J. Sanjayan, F. Collins, Phase transformations and mechanical

strength of OPC/Slag pastes submitted to high temperatures, Mater Struct 41 (2008) 345-350

[75] J. Temuujin, W. Rickard, M. Lee, A. van Riessen, Preparation of metakaolin based geopolymer coatings on metal substrates as thermal barriers, J Non-Cryst Solids 357 (2011) 1399-1404

[76] P. Duxson, G.C. Lukey, J.S.J. Van Deventer, Thermal evolution of metakaolin geopolymers: Part 1 – Physical evolution, J Non-Cryst Solids 352 (2006) 5541-5555

[77] P. Duxson, G.C. Lukey, J.S.J. Van Deventer, Thermal evolution of metakaolin geopolymers: Part 2 – Phase stability and structural development, J Non-Cryst Solids 353 (2007) 2186-2200

[78] M. Merlini, M. Gemmi, G. Artioli, Thermal expansion and phase transitions in akermanite and gehlenite, Phys Chem Miner 32 (2005) 189-196

[79] R.M. Weston, P.S. Rogers, Anisotropic thermal expansion characteristics of wollastonit,. Mineral Mag 40 (1976) 649-651

[80] G.L. Hovis, J. Crelling, D. Wattles, B. Dreibelbis, A. Dennison, M. Keohane, S. Brennan, Thermal expansion of nepheline-kalsilite crystalline solutions, Mineral Mag 67 (2003) 535-546

[81] M. Tribaudino, R.J. Angel, F. Camara, F. Nestola, D. Pasqual, I. Margiolaki, Thermal expansion of plagioclase feldspars, Contrib Mineral Petr 160 (2010) 899-908

[82] M.C. Bignozzi, S. Bonduà, Alternative blended cement with ceramic residues:

Corrosion resistance investigation on reinforced mortar, Cement Concrete Res 41 (2011) 947–954

[83] J.B. Newman, B.S. Choo, Advanced concrete technology, Butterworth-Heinemann ed. (2003), Oxford, GB, pp. 352

[84] K.E. Curtis, K. Mehta, A critical review of deterioration of concrete due to corrosion of reinforcing steel, Proceedings of Fourth CANMET/ACI Int. Conf. (1997) Sydney, Australia

[85] Y. Muntingh, Durability and diffusive behaviour evaluation of geopolymeric material, PhD thesis (2006) Stellenbosh University, South Africa